Deuteron breakup $pd \rightarrow \{pp\}_s n$ with forward emission of a fast $^1S_0$ diproton

S. Dymov,[1,2] V. Komarov,[2] G. Macharashvili,[2] Yu. Uzikov,[2] T. Azarian,[2] O. Imambekov,[2,3] A. Kulikov,[2] V. Kurbatov,[2]
S. Merzliakov,[2] B. Zalikhanov,[2] N. Zhuravlev,[2] M. Büscher,[4] M. Hartmann,[4] V. Hejny,[4] A. Kacharava,[4] M. Nekipelov,[4]
H. Ohm,[4] F. Rathmann,[4] H. Seyfarth,[4] H. J. Stein,[4] H. Ströher,[4] A. Khoukaz,[5] T. Mersmann,[5] T. Rausmann,[5] S. Barsov,[6]
S. Mikirtychiants,[4,6] B. Kämpfer,[7] P. Kulessa,[8] M. Nioradze,[9] S. Trusov,[7,10] and S. Yaschenko[1,2,*]

[1]*Physikalisches Institut, Universität Erlangen-Nürnberg, D-91058 Erlangen, Germany*
[2]*Laboratory of Nuclear Problems, JINR, RU-141980 Dubna, Russia*
[3]*Kazakh National University, KZ-050038, Almaty, Kazakhstan*
[4]*Institut für Kernphysik and Jülich Centre for Hadron Physics, Forschungszentrum Jülich, D-52425 Jülich, Germany*
[5]*Institut für Kernphysik, Universität Münster, D-48149 Münster, Germany*
[6]*High Energy Physics Department, Petersburg Nuclear Physics Institute, RU-188350 Gatchina, Russia*
[7]*Hadron Physics Division of Forschungszentrum Dresden Rossendorf, D-01328 Dresden, Germany*
[8]*H. Niewodniczanski Institute of Nuclear Physics PAN, PL-31342 Cracow, Poland*
[9]*High Energy Physics Institute, Tbilisi State University, 0186 Tbilisi, Georgia*
[10]*Skobeltsyn Institute of Nuclear Physics of Lomonosov Moscow State University, Moscow, RU-119991, Russia*

The deuteron breakup reaction $pd \rightarrow \{pp\}_s n$, where $\{pp\}_s$ is a fast proton pair emitted in forward direction with small excitation energy $E_{pp} < 3$ MeV, has been studied at proton beam energies of 0.5–2.0 GeV using the ANKE spectrometer at COSY-Jülich. The differential c.m. cross sections are measured in complete kinematics and provide angular distributions of the neutron emission angle in the range $\theta_n = 168°–180°$, the dependence on beam energy at $\theta_n = 180°$, angular distributions of the direction of the proton in the pp rest frame, and distributions of the excitation energy E_{pp} of the proton pair. The obtained data are analyzed on the basis of theoretical models previously developed for the $pd \rightarrow dp$ process in a similar kinematics and properly modified for the diproton channel in $pd \rightarrow \{pp\}_s n$. It is shown that the measured observables are highly sensitive to the short-range part of the nucleon-nucleon interaction.

I. INTRODUCTION

The structure of the lightest nuclei at short distances ($r_{NN} < 0.5$ fm) or high relative momenta ($q > 1/r_{NN} \sim 0.4$ GeV/c) and the closely related nucleon-nucleon (NN) interaction constitute fundamental problems in nuclear physics. Electromagnetic probes are generally considered the cleanest approach for these investigations and most of our knowledge about the short-range structure of the deuteron was obtained from elastic electron-deuteron scattering [1,2]. With increasing transferred momentum Q, however, the theoretical interpretation of electromagnetic processes becomes less clear due to meson-exchange currents, whose strength, related to the strong interaction, is not well established. At photon energies above 1 GeV at large angles in the c.m., the meson-exchange picture fails to explain, e.g., deuteron photodisintegration data on $\gamma d \rightarrow pn$ [1,3], because internal hadronic degrees of freedom become essential and new physics mechanisms come into play.

Independent information about the short-range structure of nuclei can be obtained from hadronic processes at large Q. The existing data in deep-inelastic reactions $h + A \rightarrow p + X$ in the so-called cumulative region with a final proton emitted into the backward hemisphere are often treated in terms of interactions with density fluctuations of cold nuclear matter

[4,5] or short-range NN correlations in nuclei [6], whose local properties are considered to be largely independent of the type of nucleus A and the used probe h. Because of the complicated structure of the involved nuclei and initial- and final-state interactions in the nuclear medium, the analysis of such processes presents quite a challenge to theory [7]. It is therefore important to study elementary processes in few-nucleon systems that probe the short-range NN interaction under conditions that make the theoretical interpretation more transparent by suppressing less well-constrained contributions.

Investigations of the simplest processes in the GeV region with high transferred momentum, that is, proton-deuteron backward elastic scattering $pd \rightarrow dp$ [8,9] and inclusive $dp \rightarrow p(0°)X$ [10–12] deuteron disintegration turned out to be inconclusive with respect to the short-range interaction. Below the pion threshold, differential cross sections, tensor analyzing powers T_{20}, and spin-transfer coefficients κ in the $pd \rightarrow dp$ and $dp \rightarrow p(0°)X$ reactions are reasonably well described by quasifree approximations [13]. These are based on one-nucleon exchange (ONE) where the external proton interacts with one nucleon in the deuteron, while the second nucleon acts as a spectator, whose momentum $\vec{q}$ in the deuteron rest frame is opposite to the momentum of the incident proton. In the ONE mechanism the unpolarized cross section is proportional to $u^2(q) + w^2(q)$, where $u(q)$ and $w(q)$ denote the S- and D-wave components of the deuteron wave

function at internal momentum q. T_{20} and κ are completely determined by the ratio w/u [13]. Within the ONE mechanism the aforementioned observables directly measure the nucleon momentum distribution in the deuteron. At energies above the Δ-isobar threshold, where internal momenta inside the deuteron above $0.3 \, \text{GeV}/c$ are probed, the quasifree ONE approximation fails to explain the existing data. Except for the Δ region (0.8–1.2 GeV) in dp collisions, the ONE model calculations with the Paris [14] and Reid soft core (RSC) [15] wave function of the deuteron are in rough agreement with the unpolarized cross sections of the $dp \rightarrow p(0°)X$ and $pd \rightarrow dp$ reactions up to very large nucleon momenta $q \sim 1 \, \text{GeV}/c$ in the deuteron. However, experimental values of the tensor analyzing power T_{20} [9,16] strongly contradict the ONE model calculations already at $q > 0.3 \, \text{GeV}/c$ for any realistic NN potential. This puzzling circumstance has sometimes been treated as an indication for non-nucleonic degrees of freedom in the deuteron, but this interpretation is not compatible with the behavior of the tensor polarization T_{20} in elastic ed scattering [1,2].

The previously described disagreement in the theoretical interpretation of pd reactions can be attributed to contributions from three-body forces related to the excitation of nucleon isobars (Δ, N^*) in the intermediate state, which have been neglected in the ONE analyses [9–12]. The Δ mechanism dominates the large-angle unpolarized $pd \rightarrow dp$ cross section at 0.4–0.6 GeV [17–19]. The spin structure of the three-body forces related to the Δ isobar is far from being established [20], and this leads to ambiguities in the explanation of T_{20} when the Δ isobar is included in the transition amplitude [17–19]. Above the $\Delta(1232)$ region the contribution of heavier baryon resonances is expected to increase and the theoretical interpretation of this process becomes much more uncertain.

In view of these difficulties it would be highly desirable to study a process kinematically similar to $pd \rightarrow dp$ scattering, where contributions from the excitation of Δ and N^* resonances are suppressed. For that purpose, it was suggested [21–23] to study the reaction

$$p + d \rightarrow \{pp\}_s + n, \qquad (1)$$
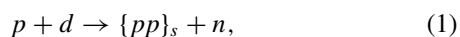
where $\{pp\}_s$ is a proton pair at small excitation energy ($E_{pp} < 3 \, \text{MeV}$) emitted in a forward direction. The kinematics of this reaction is very similar to that of pd backward elastic scattering. Hence, the same mechanisms can be applied in the analysis of the deuteron breakup with a diproton in the final state [Eq. (1)]. The restriction to $E_{pp} < 3 \, \text{MeV}$ at high transferred momentum Q assures that the diproton is in a $^1S_0$ state, in contrast to the $^3S_1$-$^3D_1$ state of the deuteron. This difference changes the relative contributions of the involved mechanisms to the reaction amplitude. Due to isospin invariance, the contribution of the excitation of a Δ resonance to the cross section is reduced by a factor of 9 in the $pd \rightarrow \{pp\}_s n$ reaction compared to that of pd backward elastic scattering [24]. The same suppression factor also applies for other isovector excitations, such as N^* resonances, whereas the ONE mechanism does not suffer a similar suppression [24]. Furthermore, compared to $dp \rightarrow p(0°)X$ and pd backward elastic scattering, the ONE mechanism of the $pd \rightarrow \{pp\}_s n$

reaction is strongly modified due to the NN repulsive core. This leads to a node of the NN ($^1S_0$) scattering amplitude at off-shell momenta $q' \sim 0.4 \, \text{GeV}/c$ [21,22]. In the $pd \rightarrow dp$ and $dp \rightarrow p(0°)X$ reactions, the corresponding node of the S-wave deuteron wave function is hidden by the large D-wave contribution. The contribution of the ONE mechanism, highly sensitive to the NN potential at short distances, should show a very different energy dependence in the deuteron breakup with a diproton in the final state compared to pd backward elastic scattering. Therefore, due to substantial modifications of the dominant terms in the transition amplitude, the $pd \rightarrow \{pp\}_s n$ reaction might allow one to obtain a better understanding of the relative importance of contributions from ONE and (Δ, N^*) excitations.

The first measurements of the unpolarized differential cross section of the deuteron breakup with a diproton in the final state was performed at beam energies in the range of 0.6–1.9 GeV [25]. The theoretical analysis of the data is described in Ref. [26] using an approach, originally suggested for pd backward elastic scattering [17], properly modified for the diproton channel [21] and taking into account initial- and final-state interactions [23]. When employing a modern high-accuracy NN potential, for example, CD-Bonn [27], a reasonable agreement with the data of Ref. [25] is obtained [26], while harder NN potentials like the Paris or the RSC potential strongly contradict the data. The interpretation is that these potentials generate high-momentum components of the NN-wave function that are too intense and this leads to large ONE contributions, in particular at energies above 1 GeV. This is the most important finding of the analysis of the $pd \rightarrow \{pp\}_s n$ data [26].

The existing data [25] on unpolarized cross sections are not yet sufficient in regions critical for the aforementioned theoretical observation. Above 1 GeV only two data points of the differential cross section in $pd \rightarrow \{pp\}_s n$ were obtained (at 1.35 and 1.90 GeV [25]), but this region is most crucial for the discrimination between soft and hard NN potentials. Furthermore, the experimental uncertainties at those energies were rather large due to small statistics. For the same reason, it was impossible to obtain the angular dependence of the differential cross section as function of the neutron c.m. angle θ_n, which is also sensitive to the reaction mechanism.

The goal of the present work is to remedy these shortcomings. In the present article we report on new high-statistics data of the unpolarized differential cross section of the deuteron breakup reaction $pd \rightarrow \{pp\}_s n$ in the slightly extended energy range of 0.5–2.0 GeV compared to those discussed in Ref. [25]. The earlier data at proton beam energies of 0.6, 0.7, 0.8, 0.95, 1.35, and 1.90 GeV [25] are supplemented here by measurements at energies of 0.5, 0.8, 1.1, 1.4, and 1.97 GeV. Higher statistics allowed us to measure the dependence of the cross section on the neutron c.m. scattering angle θ_n and to obtain the dependence on E_{pp}, which is important to verify that the proton pair is in a $^1S_0$ state.

The article is organized as follows. The measurements and the data processing are described in Sec. II. The results are presented in Sec. III. A comparison to theory is given in Sec. IV, while Sec. V summarizes the article. The contribution of P waves to ONE is discussed in the Appendix.

II. MEASUREMENTS

A. Experimental setup

The experiment was carried out at the magnet spectrometer ANKE [28] at the internal beam of the cooler synchrotron (COSY) [29] in Jülich (Fig. 1).The magnet system of ANKE comprises three dipole magnets: the spectrometer magnet D2 for momentum analysis of the reaction products, and the deflection magnets D1 and D3 that guide the circulating beam onto the target and back to the nominal orbit.

At the beam energies T_p ranging from 0.5 to 2.0 GeV about 3×10^{10} protons could be stored in the ring. The beam had a momentum spread of $\Delta p/p \sim 10^{-3}$ and the root mean squared (rms) beam size amounted to 0.8 (1.3) mm vertically and 1.7 (2.5) mm horizontally for $T_p = 2.0$ (0.5) GeV. The cluster-jet target [30] produced a vertically directed deuterium jet with an average target thickness of 2×10^{14} atoms/cm^2 and a width of about 10 mm at the interaction point. For calibration measurements, a hydrogen jet was used as well. Positively charged secondaries produced in the target leave the D2 vacuum chamber through a 0.5-mm-thick aluminum exit window and enter the FD comprising a set of multiwire proportional chambers (MWPC) and a hodoscope consisting of two planes of counters with vertically oriented scintillators. Each MWPC includes vertically and horizontally oriented wire and inclined strip coordinate planes [31]. The tracking system provides a sufficiently high momentum resolution $\Delta p/p$ for protons from the deuteron breakup reaction [Eq. (1)]. The typical detector resolutions are listed in Table I.

The FD scintillation hodoscope provided triggering of the data acquisition system, timing for two-particle events, and energy loss measurements. The energy losses were measured with an accuracy of 11–17% (FWHM); the resolution $\sigma_{\Delta t}$ of the time difference between signals in different counters was 0.1–0.3 ns. The hodoscope allowed us also to estimate the vertical hit coordinate with a precision of 1.5–2.2 cm

TABLE I. Typical FD resolutions for protons from the deuteron breakup reaction [Eq. (1)] for the range of beam energies T_p covered in the experiment: average momentum of the detected protons $\langle p \rangle$, momentum resolution $\frac{\sigma_{\langle p \rangle}}{\langle p \rangle}$, time resolution $\sigma_{\Delta t}$ for the detection of proton pairs, and precision σ_Y of the reconstructed vertical coordinate at the target position.

	T_p (GeV)				
	0.5	0.8	1.1	1.4	1.97
$\langle p \rangle$ (GeV/c)	0.69	0.9	1.1	1.3	1.61
$\frac{\sigma_{\langle p \rangle}}{\langle p \rangle}$ (%)	1.6	1.2	1.1	1.0	0.9
$\sigma_{\Delta t}$ (ns)	0.29	0.16	0.13	0.12	0.11
σ_Y (cm)	1.2	0.93	0.77	0.71	0.62

(rms) by comparison of the time difference of signals from photomultipliers on opposite ends of the counters.

Two types of triggers were applied in parallel. The first trigger was produced by any charged particle crossing two planes of the hodoscope (single-particle or FD trigger). The second trigger (double-particle or DP trigger) employed a dedicated electronic unit which suppressed a major part of single-particle events, retaining only events with two charged particles in the FD [32]. A DP trigger was generated either when in both scintillator walls two counters were hit or when the energy loss in a single counter amounted to twice the energy loss of a single proton. In 99.8% of the FD-trigger events, a single particle was recorded and only the remainder were double-particle events. The use of the DP trigger increased the fraction of double-particle events in the recorded data by about a factor of 10.

The angular acceptance of the FD is limited to forward angles close to zero degree. The vertical acceptance covers angles $\theta_{yz} = \pm 3.5°$, and the horizontal acceptance, depending on the particle momentum, is within $\theta_{xz} = \pm 12°$ (see Fig. 2), where θ_{xz} and θ_{yz} are the projections of the particle laboratory
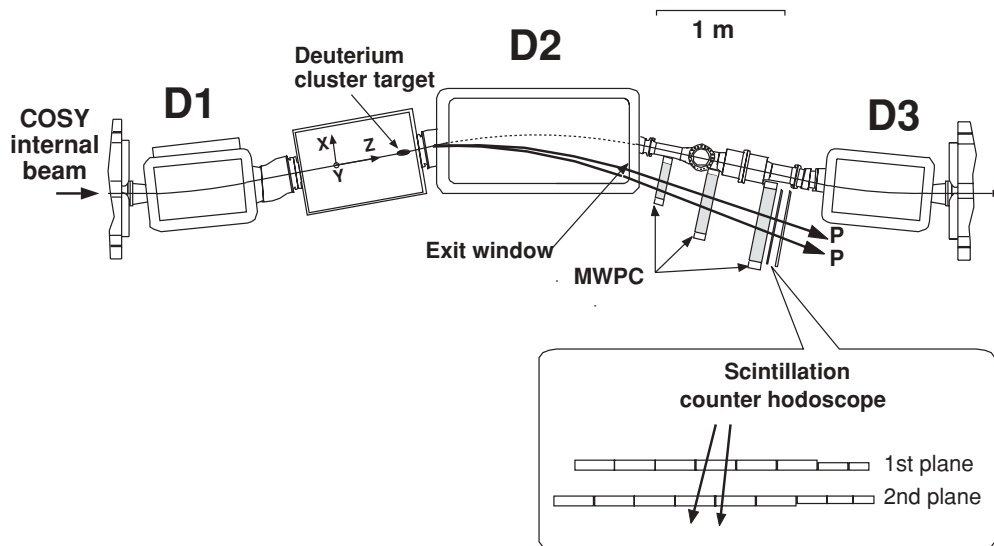

FIG. 1. Top view of the ANKE setup at COSY, showing the components used in the present experiment. The positions of the dipole magnets D1, D2, and D3; the cluster target spot; and the forward detector system (FD) are shown. The xyz coordinate system is indicated.
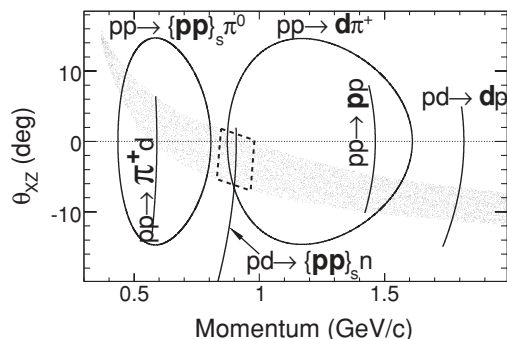
FIG. 2. Single-particle acceptance of the ANKE forward detector at $T_p = 0.8$ GeV, showing the polar angle projection θ_{xz} as a function of particle momentum. The curves show the kinematical loci for different processes (the detected particles are labeled in boldface). For the $pd \rightarrow \{pp\}_s n$ reaction, the dashed box corresponds to $E_{pp} < 3$ MeV and the solid curve is for $E_{pp} = 0$.

emission angle onto the xz and yz planes, respectively. The coordinate frame is indicated in Fig. 1, the x axis is oriented horizontally outward of the COSY ring, y is vertically up, and z is along the beam direction.

The smallest momentum accepted by the FD is $\sim 0.3p_0$, where p_0 is the beam momentum. As shown in Fig. 2, proton pairs from the breakup process with $E_{pp} < 3$ MeV are accepted at laboratory polar angles up to $\sim 7°$. The FD acceptance allows for the detection of particles from other processes ($pd \rightarrow dp$, $pp \rightarrow pp$, and $pp \rightarrow d\pi^+$), which were recorded for calibration purposes.

B. Data taking

To minimize systematic uncertainties, the geometrical arrangement of the spectrometer was the same in all three runs and at all energies. The angle of the beam deflection in D1 was fixed (at $7.4°$) and only the magnetic field in the dipoles was changed according to the beam energy. The first run was carried out at energies 0.6, 0.7, 0.8, 0.95, 1.35, and 1.9 GeV; the results are published in Ref. [25]. In the second run, data were taken at 0.5 GeV beam energy. The main part of data was collected in a third run at 0.5, 0.8, 1.1, 1.4, and 1.97 GeV. In the last run at 0.5 and 0.8 GeV a polarized beam was employed and the analyzing powers of the $\vec{p}d \rightarrow \{pp\}_s n$ reaction are reported in Ref. [33].

The luminosities at the different energies ranged from 4 to 6×10^{29} cm^{-2} s^{-1} in the first run, and were increased to 7 to 13×10^{30} cm^{-2} s^{-1} in the third one. Measurements with an H$_2$ target were carried out for calibration purposes in each of the runs.

C. Event reconstruction

Data processing included procedures of track finding and ejectile momentum reconstruction. In addition, calibrated energy losses and time information from the scintillation hodoscope were obtained [31,34].

Because the distortions of the particle trajectories in the magnetic fringe field of D2 and multiple scattering in the detector materials are small, a straight-line approximation was used to reconstruct the tracks in the MWPC region. Each of the three MWPCs measured both horizontal and vertical track coordinates, which provided an overdetermination of the straight line. This allowed us to estimate the efficiency of each chamber from the experimental data by excluding one of the chambers from the track search. The same feature allowed us also to reduce the effect of MWPC inefficiencies in the track search, since not all planes of the MWPCs are required to reconstruct the tracks. The MWPC efficiency was obtained prior to the main event reconstruction and was used to estimate the quality of the track candidates during the track search procedure.

Special attention was paid in the track finding procedure to provide a high efficiency for the reconstruction of pairs of tracks located close to each other in space. The algorithm provided about 90% reconstruction efficiency for proton pairs with E_{pp} above 1 MeV, decreasing to 75% at $E_{pp} = 0.2$ MeV [31]. The efficiency of the single-track search was 99.5%.

The reconstructed trajectories had to pass various background rejection criteria, which suppressed $\sim 40\%$ of the events taken with the FD trigger. One of the criteria used was that the track had to pass the exit window of the D2 chamber. Another criterion made use of the smallness of the nonvertical components of the D2 magnetic field. Trajectories originating from the interaction point possess a strong correlation of the vertical track coordinate with the track angle in the yz plane. This correlation, after a small correction to the magnetic field, allowed us to estimate the y coordinate of the track at the target position. The distribution of this coordinate shows a clean peak of beam-target interactions. The associated uncertainties σ_Y for events from the deuteron breakup reaction are listed in Table I. The background level under the peak amounted to less than 1% for pp elastic scattering and to about 5% for the deuteron breakup reaction.

The magnetic field of D2 was measured on a three-dimensional grid. Tracing in the magnetic fields by the Runge-Kutta method or a polynomial method was used to reconstruct the ejectile momenta. In the latter method, the components of the ejectile momenta were expressed as third-order polynomial functions of the measured track parameters, where the coefficients of the polynomials were obtained from a simulation.

The energy losses and the timing information obtained from the hodoscope [34] were calibrated. The reconstructed particle momenta were fine tuned [31] by slightly varying the geometrical parameters of the experimental setup until the nominal missing masses of processes with only one undetected particle in the final state were well reproduced (e.g., $pp \rightarrow pp$, $pp \rightarrow d\pi^+$, and $pp \rightarrow pn\pi^+$). After fine tuning of the geometry, the missing mass for protons from pp elastic scattering, for instance, differed from its nominal value by less than 0.4% at all energies. The achieved accuracy of the alignment guaranteed negligible systematic uncertainties in the determination of the kinematical parameters of the events and of the detector acceptance.

D. Resolution, efficiency, and acceptance

The momentum resolution of the experimental setup was studied by a GEANT-based Monte-Carlo simulation [35]. In the simulation the particles were traced through the setup
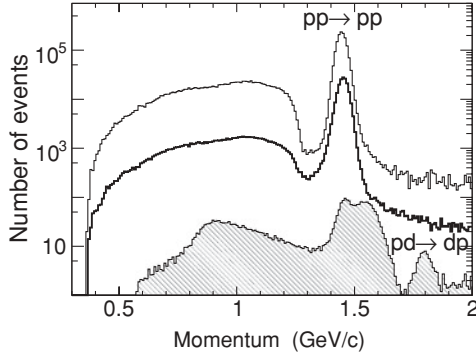
FIG. 3. Recorded momentum distributions at $T_p = 0.8$ GeV: protons with H_2 target (thin line), protons with D_2 target (thick line), deuterons with D_2 target (filled histogram). (The relative normalization of the distributions is arbitrary.)

taking into account multiple scattering, nuclear interactions in the materials, and dispersion of the hits in the MWPC. The obtained coordinates, together with admixed noise hits, were analyzed by the track reconstruction algorithm.

In the case of pp elastic scattering, the resolution obtained from the simulation could be directly compared to the width of the observed momentum distribution, taken at fixed polar angles. This comparison exhibits good agreement between simulated and experimental resolutions [31]. In Fig. 3, the momentum distributions at $T_p = 0.8$ GeV recorded with H_2 and D_2 targets are shown; pp elastic events exhibit a peak in the $(5°–10°)$ scattering angle range.

Similar simulations for the $pd \rightarrow \{pp\}_s n$ reaction allowed us to determine the resolution of single-particle momenta (see Table I), as well as the resolution of all kinematical variables $\xi \equiv (\theta_{pp}, \phi_{pp}, \theta_k, \phi_k, E_{pp})$ necessary to describe the reaction. θ_{pp} and ϕ_{pp} are the polar and azimuthal angles of the total proton pair momentum $\mathbf{P}_{pp} = \mathbf{P}_1 + \mathbf{P}_2$, where $\mathbf{P}_1$ and $\mathbf{P}_2$ denote the proton c.m. momenta (see Fig. 4). The azimuthal angle ϕ_{pp} is the angle between the direction of the x axis of the coordinate frame (see Fig. 1) and the projection of the momentum $\mathbf{P}_{pp}$ onto the xy plane. Polar and azimuthal angles of the neutron in the $pd \rightarrow \{pp\}_s n$ reaction are given by $\theta_n = 180° - \theta_{pp}$ and $\phi_n = \phi_{pp} + 180°$, respectively. Polar and azimuthal angles θ_k and ϕ_k in the rest frame of the proton pair are defined in Fig. 4 (lower panel). The kinetic energy in the rest frame of the proton pair is given by $E_{pp} = 2(m_p^2 + \mathbf{k}^2)^{1/2} - 2m_p$.

The E_{pp} resolution, shown in Fig. 5, is sufficient not only to extract pairs with $E_{pp} < 3$ MeV, but allows also the measurement of the E_{pp} distribution in this region. In the angular interval $\theta_{pp} = 15°–20°$, the rms resolution of θ_{pp} is about 0.2°; for $\theta_{pp} = 5°$ it amounts to ∼0.1°.

The FD acceptance was calculated using the same simulation program. Events of the pd interaction were generated according to the phase-space distribution for the breakup process taking into account the final-state interaction for the proton pairs. The ratio of the reconstructed to generated events was taken as the acceptance factor in each bin of the ξ space. In most cases it was possible to restrict the consideration to two-dimensional maps in $\cos \theta_{pp}$ and E_{pp},
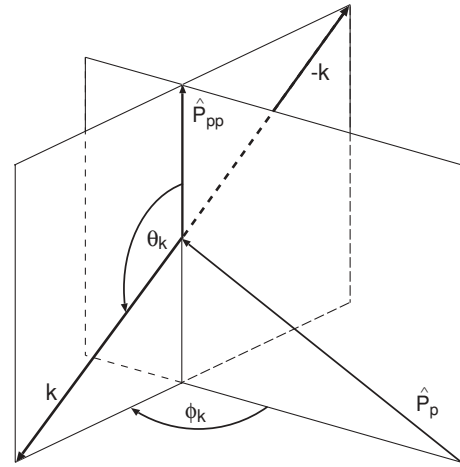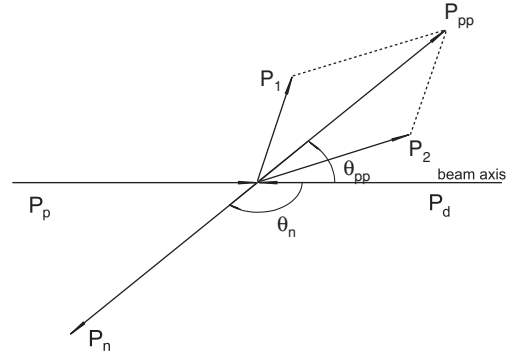

FIG. 4. Upper panel: Kinematics of the $pd \rightarrow \{pp\}_s n$ reaction in the pd c.m. system. Lower panel: $\hat{P}_p$ and $\hat{P}_{pp}$ denote the directions of the incoming beam proton and the outgoing proton pair, respectively. In the rest frame of the proton pair, protons have the momenta $\mathbf{k}$ and $-\mathbf{k}$; polar and azimuthal angles θ_k and ϕ_k are indicated.

since the distribution of other parameters could be taken to be uniform. An example of such a map is shown in Fig. 6. The acceptance factor is close to unity at the point ($E_{pp} = 0$, $\cos \theta_{pp} = 1$); it steeply drops with increasing E_{pp} and θ_{pp} due to the geometry of the setup. To check the homogeneity and to obtain distributions of ϕ_{pp}, θ_k, and ϕ_k, the acceptance was calculated as a function of each of these variables, that is, $A(\theta_{pp}, E_{pp}, \phi_{pp})$, $A(\theta_{pp}, E_{pp}, \theta_k)$, and $A(\theta_{pp}, E_{pp}, \phi_k)$. It should be noted that the calculation of the acceptance factors
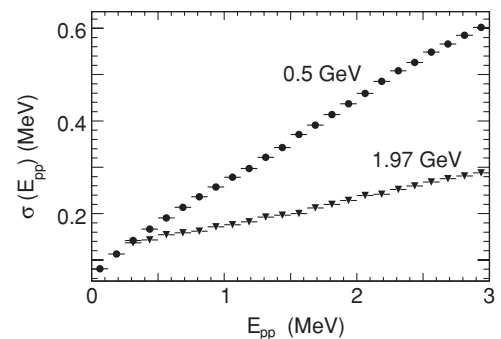

FIG. 5. Resolution of the kinetic energy E_{pp} of proton pairs, obtained from a simulation.
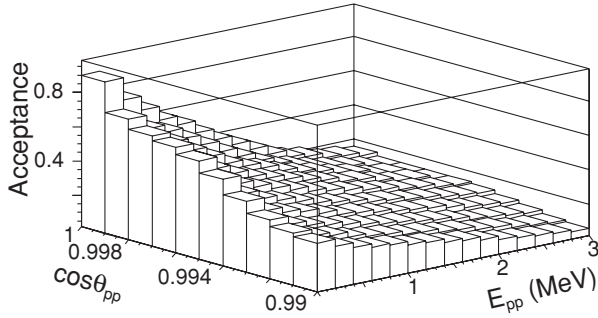
FIG. 6. Two-dimensional acceptance factor $A(\theta_{pp}, E_{pp})$ at $T_p = 0.6$ GeV.

takes into account the angular and momentum resolutions of the setup and thus the migration of events between adjacent bins of the ξ space. The calculation includes also inefficiencies of the MWPCs and of the track reconstruction algorithm. The efficiency of the hodoscope was close to 98% and was taken into account separately.

E. Identification of the reaction

The main criterion for the identification of proton pairs was based on the time information from the hodoscope. For events with two particles hitting different counters in at least one of the hodoscope planes, the time-of-flight differences from the target $\Delta t_{\rm meas}$ can be determined. Using the measured particle momenta $\vec{p}_1$ and $\vec{p}_2$ and assuming that the involved particles are protons, $\Delta t_{\rm meas}$ can be compared to $\Delta t_{\rm calc} = \Delta t(\vec{p}_1, \vec{p}_2)$. In Fig. 7, $\Delta t_{\rm meas}$ is plotted vs $\Delta t_{\rm calc}$. While proton pairs populate the line at $\Delta t_{\rm meas} = \Delta t_{\rm calc}$, pairs of particles with other masses show different distinct loci. This time-of-flight (Δt) criterion could be applied to about 85% of all two-track events in the vicinity of the neutron mass (see Fig. 8).
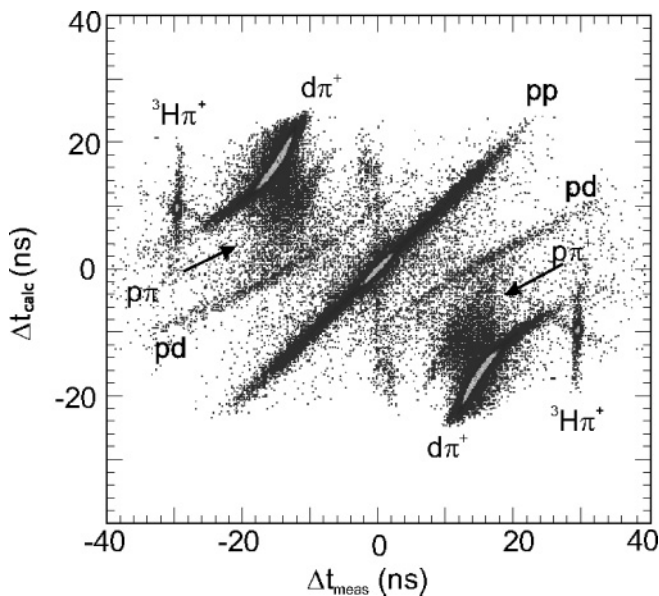

FIG. 7. Distribution of double-particle events showing the measured $\Delta t_{\rm meas}$ vs the calculated time differences $\Delta t_{\rm calc}$ at $T_p = 0.5$ GeV.
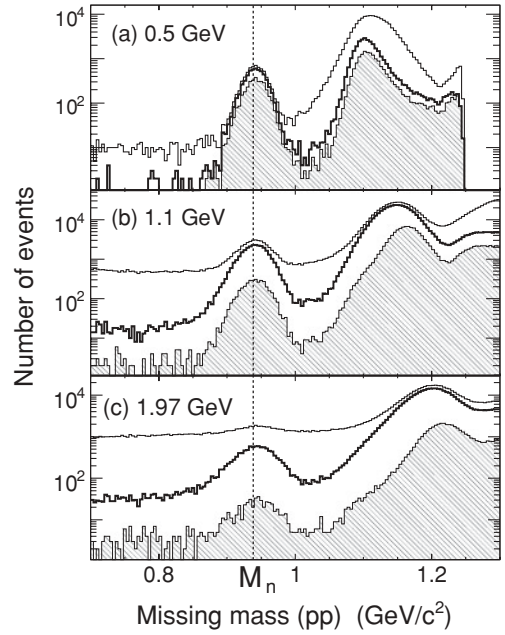

FIG. 8. Missing-mass distributions of two-particle events at three beam energies. The thin line shows all events, the thick line corresponds to proton pairs selected by the time-difference Δt criterion (Fig. 7), and the filled histograms show proton pairs with $E_{pp} < 3$ MeV.

The resolution $\sigma_{\Delta t}$ of the time differences $(\Delta t_{\rm meas} - \Delta t_{\rm calc})/\sqrt{2}$ is listed in Table I. A $2\sigma_{\Delta t}$ cut was applied that suppressed the admixture of other particle pairs among the selected proton pairs to less than 1%. Accidental events constitute the dominant contribution to the background (see Table II). The acceptance calculation took into account the requirement that the two particles must hit different counters.

The distribution of the missing mass M_X from the $pd \to ppX$ process with proton pairs exhibits a distinct peak near the neutron mass at all beam energies (Fig. 8). The mean value $\langle M_X \rangle$ corresponds to neutron masses within the accuracy provided by the setup. Their values are listed in Table II. The background-to-total ratio $N_{\rm bg}/N_{\rm tot}$ in the interval $\langle M_X \rangle \pm 3\sigma^{\langle M_X \rangle}$ amounts to several percent at low energies

TABLE II. Number of all two-track events $N_{2\text{-track}}$; number of proton pairs $N_{\Delta t}$, identified using the time-difference Δt criterion; and number of proton pairs $N^{\Delta t}_{\rm 3MeV}$ with $E_{pp} < 3$ MeV and Δt criterion applied. $\langle M_X \rangle$ is the average missing mass with resolution $\sigma^{\langle M_X \rangle}$ (both in units of MeV). $N_{\rm bg}/N_{\rm tot}$ denotes the ratio of background to total.

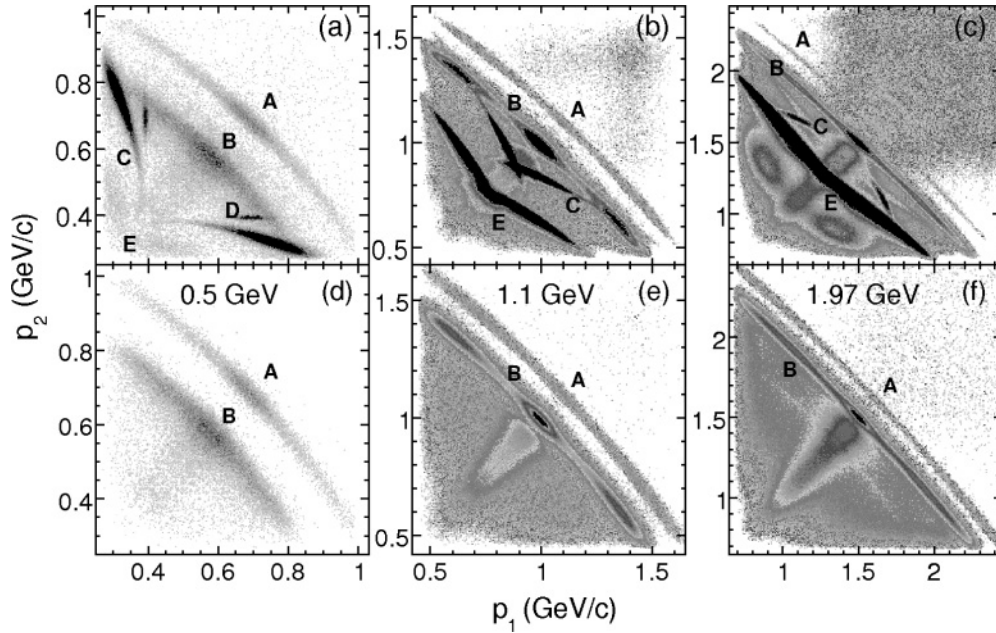| T_p (GeV)	0.5	0.8	1.10	1.40	1.97
$N_{2\text{-track}}$ (10^3)	204	1003	3119	5860	11185
$N_{\Delta t}$ (10^3)	19.6	133	800	1301	1654
$N^{\Delta t}_{\rm 3MeV}$	3417	2761	3848	1090	549
$\langle M_X \rangle$	942	942	941	940	943
$\sigma^{\langle M_X \rangle}$	16	18	20	20	24
$\frac{N_{\rm bg}}{N_{\rm tot}}$ (%)	2.0	2.7	5.2	16.5	33.6

FIG. 9. Momentum correlation of two particles detected in the FD at beam energies of 0.5, 1.1, and 1.97 GeV. Loci populated by events from the following processes are indicated: $pd \rightarrow ppn$ (A), quasifree $pN \rightarrow pp\pi$ (B), $pd \rightarrow d\pi^+ n$ (C), $pd \rightarrow {}^3H\pi^+$ (D), and quasifree $pp \rightarrow pn\pi^+$ (E). The upper panels show all pairs of particles, while the lower ones depict proton pairs selected by the time-difference Δt criterion. The distributions were symmetrized with respect to the bisecting line $p_1 = p_2$.

and increases to ∼30% at 1.97 GeV. This ratio was calculated for each bin of the relevant kinematical variables. To obtain the corresponding differential cross sections, the number of events in each bin was corrected by the acceptance factor and the background-to-total ratio for that bin. The numbers listed in Table II correspond to the most recent measurements where most of the statistics were collected. The corresponding numbers for the previous measurements are given in Table I of Ref. [25].

A different kinematical identification of two-track events is illustrated in Fig. 9. Due to kinematical restrictions caused by the narrow angular acceptance of the FD, events from processes with two or three particles in the final state populate distinct regions when particle momenta p_1 and p_2 are plotted vs each other. Protons from the deuteron breakup reaction $pd \rightarrow \{pp\}_s n$ form a narrow band. This method was only used to identify other processes, that is, B, C, D, and E in Fig. 9. For the identification of proton pairs from the $pd \rightarrow \{pp\}_s n$ reaction the missing-mass technique was applied.

F. Luminosity

Protons from elastic pd scattering and from quasielastic deuteron disintegration $pd \rightarrow pnp$ detected at small angles in the FD allowed us to determine the luminosities over a wide range of beam energies, 0.6–2.0 GeV.

At all beam energies, the proton momentum spectra exhibit a peak that is somewhat shifted from the value defined by the kinematics of elastic pp scattering (Fig. 3). The peak shape is slightly non-Gaussian on the left side, which is attributed to quasielastic deuteron disintegration. The available momentum resolution does not allow one to separate pd elastic scattering

from quasielastic deuteron disintegration. The detected events are therefore associated with the sum of elastic and inelastic cross sections, $(d\sigma/d\Omega)^{\rm el}$ and $(d\sigma/d\Omega)^{\rm inel}$, respectively. Glauber-Sitenko diffraction scattering theory [36,37] was used to calculate $(d\sigma/d\Omega)^{\rm el}$, while $(d\sigma/d\Omega)^{\rm inel}$ was obtained in closure approximation of diffraction scattering theory [36]. The parameters of pN scattering were taken from Ref. [38] and the deuteron nuclear density was taken in accordance with the S-wave component of the RSC deuteron wave function [15]. The calculation shows that the contributions of elastic and inelastic scattering are comparable at $\theta_{\rm lab} \approx 5°–10°$ in the energy range $T_p = 0.6–2.0$ GeV. The precision of the calculation for $(d\sigma/d\Omega)^{\rm el}$ was compared to known experimental data on pd elastic scattering [38–41], while the inelastic part could be only compared to data at 0.956 GeV [42]. Experimental and theoretical values were found to agree within 7% (rms), and this value was taken as normalization uncertainty for the luminosity in the range 0.6–2.0 GeV (see Appendix D of Ref. [43]).

At 0.5 GeV, the luminosity was determined in a different way. Because the precision of the calculation of $(d\sigma/d\Omega)^{\rm inel}$ degrades at energies below 0.6 GeV, only for the data obtained at 0.5 GeV was a normalization based on pd backward elastic scattering used. Deuterons detected in the FD are identified by their energy losses in the hodoscope at momenta below ∼2 GeV/c. As shown in Fig. 3, the selected deuterons produce a clean peak in the momentum distributions, and the data were normalized to the available experimental data [38,44–49] obtained under similar kinematical conditions. Based on the available data, an interpolation was carried out, using an empirical expression $(d\sigma/d\Omega)(T_p, \theta) = \exp[A(T_p)\cos\theta + B(T_p)]$ with a smooth energy dependence of the coefficients $A(T_p)$ and $B(T_p)$ in the range $T_p = 0.4–1.0$ GeV. The luminosities

TABLE III. Differential c.m. cross sections of the $pd \rightarrow \{pp\}_s n$ reaction at $\theta_n = 180°$ and averaged in the interval $\theta_n = 172°{-}180°$ in units of μb/sr. Listed also are the statistical and total uncertainties, σ^{stat} and σ^{tot}, and the integrated luminosities, L^{int}, in units of 10^{34} cm^{-2}. New data are indicated by a bullet (•).

T_p (GeV)	0.50	0.60	0.70	0.80	0.95	1.10	1.35	1.40	1.90	1.97
Refs.	•	[25]	[25]	• [25]	[25]	•	[25]	•	[25]	•
L^{int}	18.69	1.41	1.93	31.5	1.28	71.9	0.69	126.2	0.74	136.0
$\sigma^{L^{\text{int}}}$	1.80	0.12	0.17	2.4	0.11	5.9	0.06	10.5	0.07	10.9
$\frac{d\sigma}{d\Omega}(\theta_n = 180°)$	3.36	1.92	0.79	0.73	0.42	0.300	0.088	0.046	0.034	0.034
σ^{stat}	0.21	0.12	0.06	0.05	0.04	0.009	0.029	0.003	0.012	0.002
σ^{tot}	0.38	0.22	0.10	0.08	0.06	0.027	0.032	0.006	0.016	0.004
$\frac{d\sigma}{d\Omega}(\theta_n = 172°{-}180°)$	2.95	1.72	0.72	0.68	0.41	0.303	0.10	0.053	0.03	0.029
σ^{stat}	0.13	0.09	0.05	0.02	0.04	0.006	0.02	0.002	0.01	0.002
σ^{tot}	0.29	0.19	0.09	0.06	0.06	0.027	0.04	0.005	0.014	0.003

obtained this way and from the method described in the previous paragraph were compared at 0.8 GeV and were found to be consistent within 20%, which is quite reasonable since the available data at 0.8 GeV [46,49,50] agree only within 15%.

The previously described determination of the luminosity was carried out independently for different angular intervals of protons and deuterons. In all cases, the observed variation of the luminosities at different angles did not exceed 5%, and this value, taken as an additional systematic uncertainty, was included in the total uncertainty of the luminosity.

As an independent test of the luminosity determination, the quasifree $pp \rightarrow d\pi^+$ reaction was used at all energies 0.5–1.97 GeV (see Fig. 9, label C). Deuterons and pions were detected in the FD, and the neutron was identified via the missing-mass technique. The reconstructed momentum of the neutron was limited to less then 100 MeV/c; thus the neutron could be considered as a spectator. The cross section for the free $pp \rightarrow d\pi^+$ process taken at the proper c.m. energy was used for normalization. The $pp \rightarrow d\pi^+$ cross section was obtained from the SAID phase shift analysis [51] for beam energies up to 1.4 GeV, while the data of Ref. [52] were used for $T_p = 1.97$ GeV. The resulting luminosities agree within 11% with the ones obtained by the $pd \rightarrow pX$ and $pd \rightarrow dp$ processes.

III. EXPERIMENTAL RESULTS

In this section, the E_{pp} distributions of the binary reaction $pd \rightarrow \{pp\}_s n$ are presented to verify the dominance of the $^1S_0$ state in the final pp pairs for $E_{pp} < 3$ MeV. Thereafter, the obtained dependencies of the differential cross sections of the $pd \rightarrow \{pp\}_s n$ reaction on $\cos \theta_k$, $\cos \theta_n$, and T_p are presented.

A. Excitation energy E_{pp}

The excitation energy distributions have been obtained in the interval $E_{pp} = 0$–3 MeV for events with $\cos \theta_{pp} = 0.98$–1.0. The raw spectra near $E_{pp} = 0$ are distorted by the efficiency of the pair reconstruction algorithm and by migration of events caused by the resolution in E_{pp}. The two effects act in opposite directions; therefore the resulting correction in the lowest bin, ranging from 0 to 0.13 MeV, is only at the level of about 10%. The observed event distributions $N(E_{pp}, \cos \theta_{pp})$ were corrected by the two-dimensional acceptance factor $A(E_{pp}, \cos \theta_{pp})$. To avoid event losses near the upper boundary, the acceptance correction was carried out in a wider E_{pp} interval up to 7.5 MeV.

Using the Migdal-Watson final-state interaction (FSI) approach [53,54], the E_{pp} distributions were generated in the form $dN/dE_{pp} = k|M_{pp}(E_{pp})|^2$, where the momentum k comes from the phase-space factor, and the factor $|M_{pp}(E_{pp})|^2$ is given by the squared amplitude of pp scattering [55]

$$M_{pp}(E_{pp}) = e^{i\delta} \frac{\sin \delta}{k} \frac{1}{C_k}. \qquad (2)$$

Here, C_k is the Coulomb penetration factor and δ is the hadronic phase shift of $pp(^1S_0)$ scattering, modified by the Coulomb interaction.

Using the luminosities listed in Table III, the acceptance corrected distributions were converted into differential cross sections $d\sigma/dE_{pp}$, which are shown in Fig. 10. The experimental distributions clearly differ from phase space, but are satisfactorily described within the Migdal-Watson FSI approach. The data at $T_p = 1.97$ GeV are of limited accuracy and contain a substantially larger background contamination. Neither phase-space distributions nor the Migdal-Watson FSI

TABLE IV. Parameters of the $\cos \theta_k$ distributions (shown in Fig. 11) obtained from Legendre polynomial fits using Eq. (3).

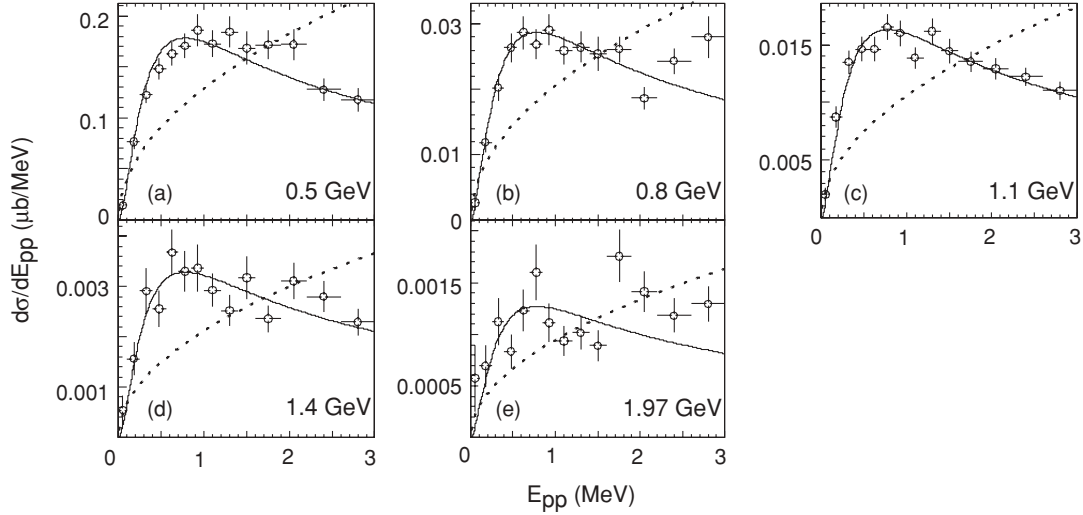| T_p (GeV)	0.5	0.8	1.1	1.4	1.97
C_2/C_0 (10^{-2})	-2.5 ± 1.0	0.6 ± 0.9	-2.0 ± 0.7	0.2 ± 1.3	0.5 ± 1.6
χ^2/ndf	6.6/8	1.6/8	5.6/8	6.6/8	10.2/8

FIG. 10. Differential cross section $d\sigma/dE_{pp}$ as a function of E_{pp}, integrated in the interval $\cos\theta_{pp} = 0.98–1$ and $\phi_{pp} = 0–2\pi$. The solid lines correspond to the Migdal-Watson approach, and the dotted lines depict phase-space distributions.

approach describe these data well. It should be noted that the Migdal-Watson FSI approximation is valid if E_{pp} is small but the transferred momentum Q is large so that the short-range part of the S wave of the internal pp motion dominates the transition amplitude [53,54]. The accuracy of the Migdal-Watson approach in describing the shape of the E_{pp} distributions was analyzed in Refs. [56,57] and was found to be about 10%. The analysis of the E_{pp} distributions in the $pd \to \{pp\}_s n$ reaction *beyond* the Migdal-Watson approximation is discussed in Sec. IV A.

B. Proton emission angle θ_k in the rest frame of the proton pair

In the framework of the Migdal-Watson FSI approach, the distribution of the proton emission angle θ_k in the c.m. system of the proton pair (Fig. 4) is determined by the amplitude of low-energy pp scattering. At energies $E_{pp} \gtrsim 0.2$ MeV, pp scattering is governed by the strong interaction in the $^1S_0$ state [58] and therefore should result in an isotropic angular distribution, except at very small angles where effects from Coulomb scattering begin to appear. The $\cos\theta_k$ distributions obtained with the three-dimensional acceptance factors $A(E_{pp}, \cos\theta_{pp}, \cos\theta_k)$ and integrated in the intervals $E_{pp} = 0–3$ MeV and $\cos\theta_{pp} = 0.98–1$ are almost isotropic, as shown in Fig. 11. The anisotropy in the pp system was estimated by fitting the distributions in even terms of Legendre polynomials up to order $l = 2$,

$$\frac{d\sigma}{d\Omega}(\theta_k) = \sum_{l=0,2} C_l(2l+1)P_l(\cos\theta_k)$$

$$= C_0\left[1 + \frac{C_2}{C_0}5\frac{(3\cos^2\theta_k - 1)}{2}\right]. \quad (3)$$

Only even Legendre polynomials P_l are included, because the differential cross section should be symmetric with respect

to the exchange of the two protons,

$$\frac{d\sigma}{d\Omega}(\theta_k) \equiv \frac{d\sigma}{d\Omega}(\pi - \theta_k).$$

The fit parameters in Table IV indicate that within statistics, negligibly small anisotropies are observed. Possible P-wave contributions to ONE are discussed in the Appendix.
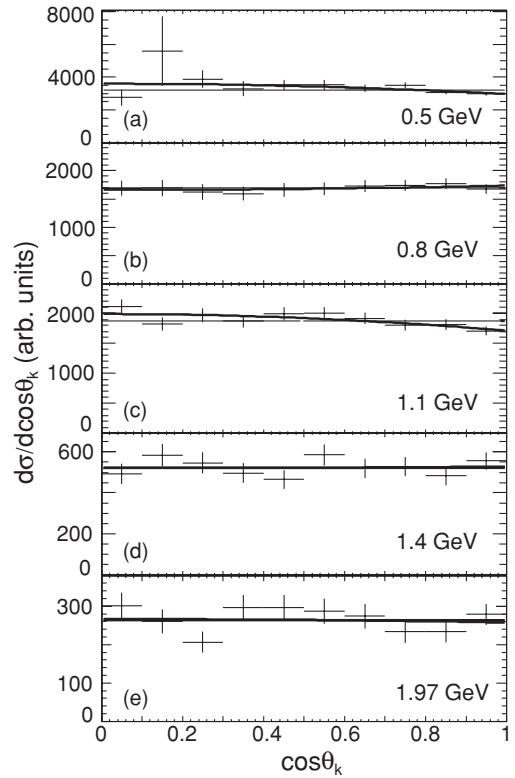

FIG. 11. Dependence of the differential c.m. cross section on $\cos\theta_k$. The curves show Legendre polynomial fits using Eq. (3); their parameters are listed in Table IV.
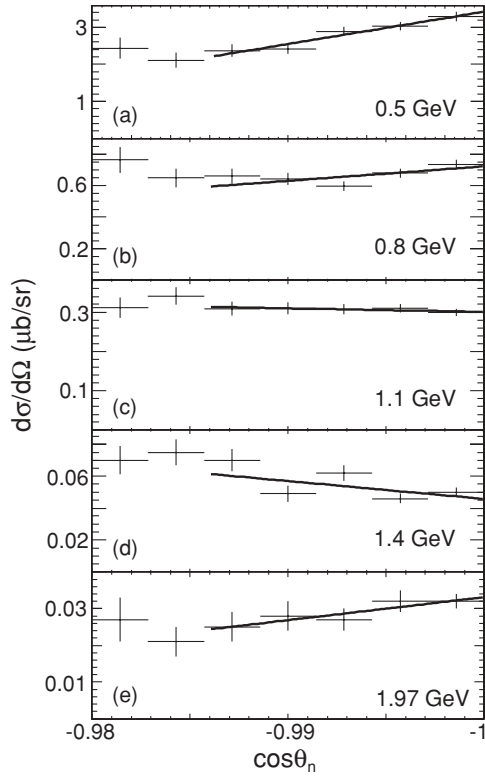
FIG. 12. Dependence of the differential c.m. cross section of the $pd \rightarrow \{pp\}_s n$ reaction on the neutron emission angle θ_n in the c.m. system for the interval $E_{pp} = 0$–3 MeV. The lines represent linear fits in the interval $\cos \theta_n = -0.985$ to -1.00.

C. Neutron emission angle $\cos \theta_n$

For the interval of neutron emission angles in the c.m., $\theta_n = 168.5°$–$180°$, the differential cross sections, integrated over E_{pp} from 0 to 3 MeV, are shown in Fig.12. The acceptance of the setup includes $\theta_n = 180°$; therefore the data allow one to obtain the differential cross section $(d\sigma/d\Omega)(\theta_n)$ exactly in a backward direction. The data were fitted by a linear function in the interval $\cos \theta_n = -0.985$ to -1.00, where the cross sections vary smoothly.

In pd elastic scattering many measurements were performed at backward proton angles $\theta_p \lesssim 170°$ [38,44–48,50]. The measured cross sections drop monotonously with decreasing proton scattering angles, exhibiting a wide backward peak. Very close to scattering angles $\theta_p = 180°$ experimental data are absent. The only comparable measurement in the angular range up to about $179°$ was carried out at 0.794 GeV in $nd \rightarrow dn$ scattering [49]. The observed angular dependence in the range $171.8°$–$178.57°$ is flat, quite similar to our measurement at 0.8 GeV (see Fig. 12).

D. Differential cross section at $\theta_n = 180°$

The differential cross sections at $\theta_n = 180°$ of the new data obtained here, of the previously published ones from Ref. [25], and of the data obtained during the measurement with polarized beam [33], for which differential cross sections were not yet published, are given in Table III. The new data and the data obained with the polarized beam allowed a direct

determination of the differential cross sections at $\theta_n = 180°$ using the measured angular distributions. Because of the limited statistics, this was not possible for the previously published ones [25], for which only the differential cross sections *averaged* in the interval $\theta_n = 172°$–$180°$ were obtained. Using the new data, the ratios of the differential cross sections at $\theta_n = 180°$ to the ones averaged over that interval were determined individually at $T_p = 0.5, 0.8, 1.1, 1.4,$ and 1.97 GeV. By interpolation, the corresponding ratios for the published data were determined, and by multiplying the previously obtained averaged cross sections with this ratio, the differential cross sections at $\theta_n = 180°$ could also be determined for these data. Differential cross sections measured during different runs at the same energies (0.5 and 0.8 GeV) agreed within errors and were weighted averaged. Data obtained with a polarized beam [33] at 0.5 and 0.8 GeV were spin averaged and otherwise treated in the same way as the new data at 1.1, 1.4, and 1.97 GeV.

The energy dependence of the cross section at $\theta_n = 180°$ is shown in Fig. 13 together with the data for pd backward elastic scattering. It should be noted that the $pd \rightarrow dp$ data are extrapolated to $180°$ due to the absence of direct measurements at this angle. In the energy range of $T_p = 0.5$–1.4 GeV, the differential cross section of the $pd \rightarrow \{pp\}_s n$ reaction drops almost exponentially with increasing energy, while in the region above ~ 1.4 GeV the energy dependence is much flatter.

The ratio of the differential cross sections of the $pd \rightarrow \{pp\}_s n$ reaction and pd backward elastic scattering amounts to $\sim 1/115$, as shown in Fig. 13. This ratio remains constant in the energy range of 0.5–2.0 GeV. Very similar results were obtained in Ref. [59] for the ratio of the differential cross sections of the $pd \rightarrow \{pn\}_s p$ and $dp \rightarrow dp$ reactions at 585 and 800 MeV for proton c.m. scattering angles ranging from $\theta = 70°$ to $120°$. As discussed in Ref. [60], the ratio of the

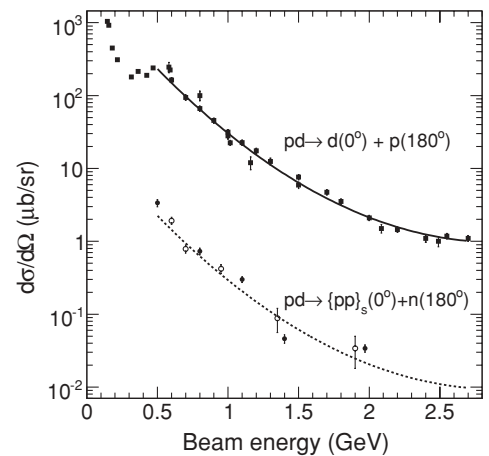FIG. 13. Energy dependence of the differential c.m. cross sections of the deuteron breakup $pd \rightarrow \{pp\}_s n$ at $\theta_n = 180°$ and of backward pd elastic scattering ([38,44–47,50] and Refs. therein). The previously obtained data of Ref. [25] are shown by open circles (○), and the new data are shown by bullets (●). The solid line represents a quadratic fit to $\log(d\sigma/d\Omega)$ of the $pd \rightarrow dp$ data, the dashed line is obtained by scaling the solid line by a factor $r = 8.8 \times 10^{-3}$, introduced in Eq. (4).

differential cross sections can be written as

$$r = \frac{\frac{d\sigma}{d\Omega}(pd \rightarrow \{pp\}_s n)}{\frac{d\sigma}{d\Omega}(pd \rightarrow dp)} = 2RZ\zeta, \qquad (4)$$

where ζ is the ratio $|A_s|^2/|A_t|^2$ of the squared reduced matrix elements of the $pd \rightarrow p(pn)_{s,t}$ reaction with an np pair in the spin-singlet (s) and triplet (t) states, as defined in Ref. [60] within the Migdal-Watson approximation. The factors R and Z are determined in Ref. [60] by the on-shell NN-scattering data at low energies. Using the values $Z = 0.101$ and $R = 2.29$, one obtains the singlet-to-triplet ratio $\zeta = (2.3 \pm 0.5) \times 10^{-2}$, $(1.6 \pm 0.3) \times 10^{-2}$, and $(2.1 \pm 1.2) \times 10^{-2}$ for 0.6, 0.7, and 1.9 GeV, respectively. The results for ζ, obtained here (Fig. 13), can be explained by the dominance of the Δ-isobar or the N^* excitation mechanism. The spin statistical factor contributes a factor of 1/3 to this ratio. The remaining difference given by a factor $\sim 6 \times 10^{-2}$ is determined by the reaction mechanism and the difference in the diproton and deuteron wave functions. Assuming the Δ-isobar excitation mechanism or, in the more general case, the isovector meson-nucleon exchange [24], one obtains the isotopic factor 1/9 [24]. With this additional factor the ratio in Eq. (4) is in agreement with the data up to a factor of ~ 2.

IV. COMPARISON TO THEORY

The theoretical analysis of hard pd collisions at energies around 1 GeV appears to be rather complicated. At high transferred momenta, corresponding to internal momenta in excess of 0.4 GeV/c, non-nucleonic degrees of freedom such as NN^*, N^*N^*, $N\Delta$, and $\Delta\Delta$ components, and possibly also multiquark components, are expected to contribute in the deuteron and diproton. These contributions are strongly model dependent. Choosing a particular reaction such as $pd \rightarrow \{pp\}_s n$ simplifies the theoretical analysis considerably. In collinear kinematics the internal momenta probed in this reaction are only moderately large ($q < 0.6$ GeV/c), and it is therefore appropriate to perform a theoretical analysis using a meson-baryon picture. The kinematics of the $pd \rightarrow \{pp\}_s n$ reaction is actually very similar to that of pd backward elastic scattering; hence it is reasonable to apply as a first step of the theoretical analysis the same reaction mechanisms [17–19].

A. ONE + SS + Δ approach

The analysis of the E_{pp} excitation energy distribution and of the energy and angular dependence of the differential cross section has been performed within a ONE + SS + Δ approximation [21,23]. The approach is based on the multistep scattering theory (Watson series). The involved Feynman diagrams are depicted in Fig. 14. Only the first terms up to two-loop diagrams were kept in the series, assuming that the contribution of higher-order terms is small at high energies. For the ONE mechanisms, plane-wave and distorted-wave Born approximations were used (abbreviated here by ONE(PWBA) $\equiv$ ONE, and ONE(DWBA). In the latter case, the rescatterings in the initial and final states were taken into account as described for the $pd \rightarrow dp$ reaction in Ref. [61]. Unlike the original Watson series, which includes only nucleons in the intermedi-
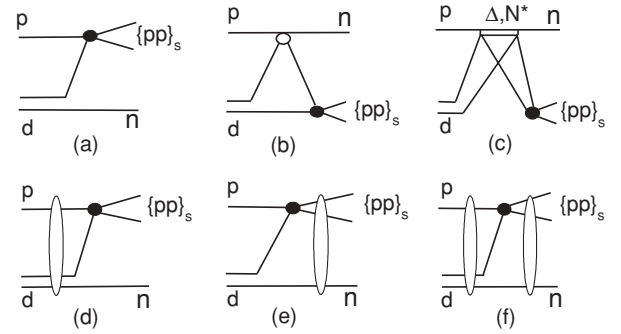

FIG. 14. Mechanisms included in the ONE + SS + Δ model of the $pd \rightarrow \{pp\}_s n$ reaction: (a) one-nucleon exchange within the plane-wave Born approximation (ONE), (b) single scattering (SS), and (c) double pN-scattering with excitation of the Δ or N* isobar (Δ). Rescatterings within the distorted-wave Born approximation (DWBA) are shown for ONE in the initial (d), final (e), and initial plus final (f) states.

ate states, possible nucleon isobars can be taken into account as well. The $\Delta(1232)$ isobar is considered explicitly. All necessary phenomenological parameters for the Δ-excitation amplitude in πN and ρN elastic scattering were determined from the data of the $pp \rightarrow pn\pi^+$ reaction at 800 MeV [62] and were described within the Δ-isobar model [63]. This allowed us to determine cut-off parameters of the monopole form factors entering at the $\pi N\Delta$ and $\rho N\Delta$ vertices, where the coupling constants were taken from Ref. [64]. The $d \rightarrow np$ and $pp \rightarrow \{pp\}_s$ vertices were determined on the basis of the Lippmann-Schwinger equation using phenomenological NN potentials. Finally, small-angle rescatterings in the initial and final states involve on-shell pN-scattering amplitudes, which were also taken from the world experimental data via a parametrization used in the Glauber theory [65]. Therefore, the ONE + SS + Δ approach used in the analysis presented here has no additional free parameters.

1. Excitation energy E_{pp}

The Migdal-Watson method, used in Sec. III A to describe the distribution of E_{pp}, was developed by making certain approximations when evaluating loop integrals, which usually appear when accounting for FSI in the reaction amplitude. An obvious advantage of the Migdal-Watson approximation is that the final result does not depend on the reaction mechanism and the type of NN interaction potential. However, if those integrals are calculated exactly for a given model of the NN interaction, this should lead to a more appropriate shape of the E_{pp} distribution as compared to the Migdal-Watson approximation for the same NN model. The only condition needed to obtain the shape of the E_{pp} dependence is that the production mechanism has to be short-ranged. In this way the precision of the Migdal-Watson approximation was tested for the case of the $pp \rightarrow NN\pi$ reaction, assuming a one-loop mechanism with virtual pion exchange [56,57]. An accounting for the FSI can be carried out also within the approach used here for the $pd \rightarrow \{pp\}_s n$ reaction. Thus, for the ONE mechanism, the E_{pp} dependence is determined by the t matrix of the half-off-shell pp scattering in the $^1S_0$ state.
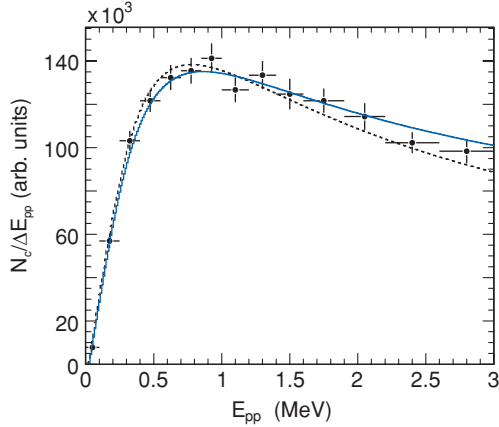
FIG. 15. (Color online) Excitation energy E_{pp} of proton pairs from the $pd \rightarrow \{pp\}_s n$ reaction. The data were summed in the interval $T_p = 0.5$–1.4 GeV. The curves show fits with the ONE + SS + Δ approximation (solid line) and the Migdal-Watson approach (dashed line).

The t matrix is given by the integral in configuration space,

$$t(q,k) = -4\pi \int_0^\infty \frac{F_0(qr)}{qr} V(r)\psi_k^{(-)*}(r)r^2 dr, \qquad (5)$$

where $\psi_k^{(-)}(r)$ is the pp scattering wave function with on-shell momentum k, $F_0(qr)$ is the regular Coulomb function for zero orbital momentum, q is the off-shell pp momentum, and $V(r)$ is the strong interaction potential in the $^1S_0$ state. The k dependence of the wave function $\psi_k^{(-)}(r)$ determines also the E_{pp} dependence of the reaction amplitude for all other mechanisms. We found numerically that the shape of the E_{pp} distribution calculated within this approach depends very little on the reaction mechanism itself. Furthermore, the theoretical result is almost independent of energy in the range 0.5–2 GeV.

To increase the statistics, the data of Fig. 10 were combined by adding the acceptance corrected number of proton pairs per E_{pp} bin in the energy interval $T_p = 0.5$–1.4 GeV. The experimental data, shown in Fig. 15, agree with the Migdal-Watson and the ONE + SS + Δ descriptions. Although the discrepancies are small, the distributions differ systematically from the Migdal-Watson ones. For the Migdal-Watson approximation, $\chi^2/\text{ndf} = 15.2/13$ (confidence level CL $= 0.29$) was obtained, and $\chi^2/\text{ndf} = 8.6/13$ (CL $= 0.80$) was obtained for the ONE + SS + Δ approximation.

2. Dependence on $\cos\theta_k$

Another way to test the dominance of the S wave in the internal state of the diproton is to study the angular dependence of the direction of the proton momentum in the c.m. system of the proton pair with respect to the total momentum of the diproton (see Fig. 4). For the $^1S_0$ state of the pp pair, this dependence is isotropic. A possible anisotropy could be produced by the admixture of states with nonzero orbital momentum $l \neq 0$ in the internal pp motion. The expected contribution of P waves to the ONE mechanism is estimated in Appendix V. The $^3P_0$, $^3P_1$, and $^3P_2$ final pp states were taken into account in addition to the $^1S_0$ state. Numerical results were obtained for the CD-Bonn NN potential. The ratio of P- to

S-wave contributions in the differential cross section is found to be $\approx 1\%$ in the range 0.5–2.0 GeV at $E_{pp} = 3$ MeV. The only exception is the vicinity of the node at 0.8 GeV, where the S-wave contribution vanishes due to the node in the half-off-shell amplitude [Eq. (5)] at $q \sim 0.4$ GeV/c, but the P-wave contribution does not. In view of the large transferred momenta in this reaction, a P-wave contribution of a few percent is expected for the SS and Δ mechanisms. Higher partial waves yield smaller contributions due to the centrifugal barrier.

The anisotropic $\cos\theta_k$ dependence in the vicinity of the ONE node for the $^1S_0$ state of the diproton, if it were observed, would directly indicate that the ONE mechanism dominates the reaction amplitude. According to the numerical calculation for the ONE mechanism alone, given in the Appendix, the anisotropic part makes up about 37% at 0.8 GeV; therefore the θ_k dependence would be strongly anisotropic. Since this is not the case, as shown in Fig. 11, the ONE mechanism clearly does not dominate at this energy.

3. Energy dependence of the differential cross section

The differential cross section of the $pd \rightarrow \{pp\}_s n$ reaction, averaged over the angular interval 172°–180°, is shown in Fig. 16 as a function of beam energy together with the results of calculations performed within the ONE(DWBA) + SS + Δ approach. The new data reported in this article are indicated by bullets ($\bullet$). The ONE mechanism alone completely fails to describe the data in the 0.5–1.5 GeV region. On the contrary, the Δ mechanism dominates in this region and its
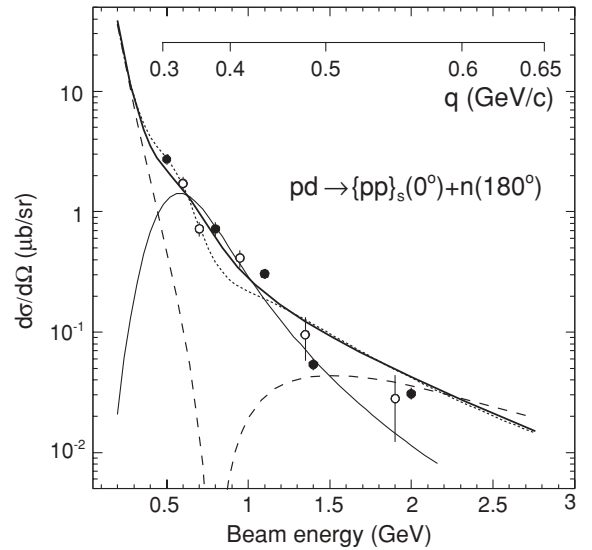

FIG. 16. Differential c.m. cross section averaged over the angular interval 172°–180° vs beam energy [26]. The curves are the result of calculations using the CD-Bonn NN potential with the ONE (dashed line) and Δ mechanisms (solid thin line), both without distortions and Coulomb effects. The ONE(DWBA) + SS + Δ is the dotted line, and the ONE(DWBA) + Δ (solid thick line) contributions are obtained with a Coulomb suppression factor of 0.83 [26]. The previously obtained data of Ref. [25] are shown by open circles ($\circ$), and the new data are shown by bullets ($\bullet$). The upper scale shows the internal momentum q of the nucleons in the deuteron for ONE at $\theta_n = 180°$.

contribution alone is sufficient to explain the gross structure of the data at 0.6–1.4 GeV. However, outside of this interval, the ONE contribution is sizable. Thus, the inclusion of the ONE mechanism below 0.6 GeV improves the agreement with the data as compared to the Δ mechanism alone. Above 1.3 GeV the Δ contribution drops quickly with increasing energy, while the ONE contribution produces a plateau in the 1.3–2.0 GeV region, smoothly decreasing with increasing energy. At these energies the ONE(DWBA) contribution also improves the agreement compared to the Δ mechanism alone, but the agreement is not as good as that at 0.5 GeV.

The sensitivity of the ONE mechanism to high-momentum components of the NN wave functions is very high, because the momenta probed in the deuteron (q) and diproton (q') for the ONE range from $q \approx q' = 0.45$ to 0.55 GeV/c for beam energies 1.4–2.0 GeV. Because of the high sensitivity, as shown in Ref. [26], those interaction potentials that are too repulsive at short NN distances $(r_{NN} < 0.6$ fm), like RSC [15] and Paris [14], strongly overestimate the cross sections of Ref. [25] at these energies within the ONE(DWBA) + SS + Δ approach. However, the results with the CD-Bonn potential were found to be in agreement with the data. The new data reported here are in agreement with this interpretation of the $pd \rightarrow \{pp\}_s n$ reaction, although overall only a qualitative agreement is achieved. In this region, heavier nucleon isobars are expected to be of minor importance; for a more detailed discussion, see Sec. IV B.

4. Angular dependence of θ_n

The results of the calculations of the angular dependence of the differential cross section are presented in Fig. 17 for
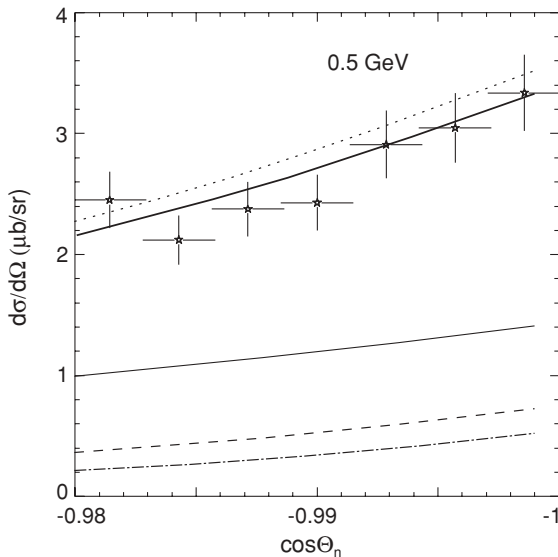

FIG. 17. Angular dependence of the differential c.m. cross section at 0.5 GeV. The curves show the results of calculations within the ONE(DWBA) + SS + Δ approach using the CD-Bonn NN potential without Coulomb interaction: ONE (dashed line), ONE(DWBA) (dashed-dotted line), Δ (solid thin line), ONE(DWBA) + SS + Δ (dotted line), and ONE(DWBA) + Δ (solid thick line). The Coulomb repulsion in the pp system, which would scale all the curves by a factor of 0.83, is not introduced here.
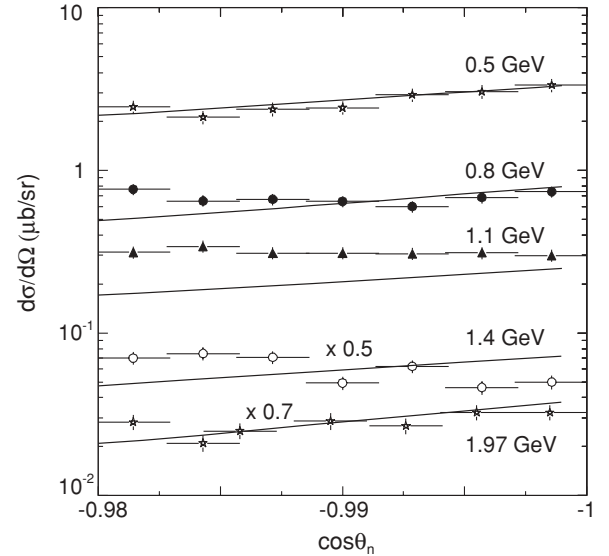

FIG. 18. Angular dependence of the differential c.m. cross section for different beam energies. The curves are for the ONE(DWBA) + SS + Δ description. The results of the calculations are scaled at 1.4 and 1.97 GeV by factors of 0.5 and 0.7, respectively. The Coulomb repulsion in the pp system, which would scale all the curves by a factor of 0.83, is not introduced here.

0.5 GeV and in Fig. 18 for the energy interval 0.5–2.0 GeV. The ONE(DWBA) yields smaller cross sections as compared to ONE. Although at 0.5 GeV this difference is rather small in magnitude, one can show that the corresponding distortion factor originating from the rescatterings in the initial and final state within the ONE(DWBA) is larger by about a factor of 2–3 at energies $T_p > 1$ GeV. Very similar results were found in pd elastic scattering within the ONE mechanism in Ref. [61]. This behavior is related to the fact that with increasing beam energy at fixed angle $\theta_n \approx 180°$ shorter distances are probed by the ONE mechanism in the deuteron (or diproton) and, therefore, this implies that rescatterings on the spectator proton become more important. Furthermore, since the elastic pN-scattering amplitudes are mainly absorptive (i.e., having large imaginary parts) at these energies, the rescatterings lead to a decrease of the reaction cross section.

At 0.5 GeV, the agreement between the ONE(DWBA) + Δ approximation and the experimental data is quite good. One should note that neither the Δ mechanism nor the ONE mechanism alone suffices to reproduce the data, underestimating the measured cross section by factors of 3 to 5, respectively. Only their coherent sum provides good agreement at this energy.

At higher energies, the theoretical description of the angular dependencies becomes worse (see Fig. 18). In general the model confirms the experimentally observed weak dependence on θ_n, but the slope and its magnitude for some energies are not well reproduced by the considered mechanisms [66]. Indeed, one can see that within the ONE(DWBA) + SS + Δ approach, the cross section smoothly increases with increasing $\cos\theta_n$ and the shape of the angular dependence changes very little in the energy range of 0.5–2.0 GeV for $-1 \leqslant \cos\theta_n \leqslant -0.98$.

The disagreement between theory and experiment at higher energies can be attributed in part to the following

factors. First, when the energy is increasing, the contributions of high-momentum components ($q > 0.3\,\text{GeV}/c$) of the two-nucleon wave function are growing, but these are not well known and depend on the choice of the NN potential used. Second, the role of absorptive rescatterings increases. In this connection, we note that in the present work (see also Ref. [26]) rescatterings in the initial and final states are taken into account within the approximation employing only the on-shell part of the singular integrals, whereas the principal value integrals (off-shell parts) are neglected. Furthermore, it is assumed in these calculations that the internal state of the diproton is not altered by rescatterings in the intermediate state. When accounting for these effects, also including a contribution from heavier nucleon resonances, one may expect to obtain a better agreement with the data in the range of 1–2 GeV.

B. OPE model

The ONE + SS + Δ approach accounts for the excitation of only one nucleon resonance, for example, the $\Delta(1232)$ isobar, because for other heavier isobars the necessary information is much more uncertain. Recently, for the description of the $pd \to \{pp\}_s n$ reaction, a one-pion exchange (OPE) model (Fig. 19) was applied [67], which takes into account the $\Delta(1232)$ contribution in pd collision in a different way compared to the ONE + Δ + SS approach. This model allows one to take into account the contribution of heavier isobars.

In one version of the OPE model, called OPE-II [67] [see Figs. 19(c) and 19(d)], the cross sections of the $pd \to dp$ and $pN \to \{pp\}_s \pi$ reactions are proportional to the pion absorption cross section on the deuteron, $\pi d \to NN$. For the unpolarized pd elastic cross section, this model is equivalent to the one previously suggested in Ref. [68]. For the $pd \to \{pp\}_s n$ reaction, the OPE-I model, shown in Fig. 19, includes the unknown coherent sum of the amplitudes of the $pp \to \{pp\}_s \pi^0$ and $pn \to \{pp\}_s \pi^-$ subprocesses. In contrast to that, the OPE-II model involves only the known subprocess $\pi^0 d \to pn$ and, therefore, its predictions are unambiguous. The OPE-II model reasonably well reproduces the differential cross sections of both reactions between 0.6 and 0.8 GeV at $\theta_n = 180°$ (see Fig. 5 of Ref. [67]). Since the $NN \to d\pi$ cross section at these energies is dominated by the $\Delta(1232)$ isobar, the obtained result, to a large extent, confirms independently the conclusion about the dominance of the $\Delta(1232)$ isobar in the $pd \to \{pp\}_s n$ reaction, found

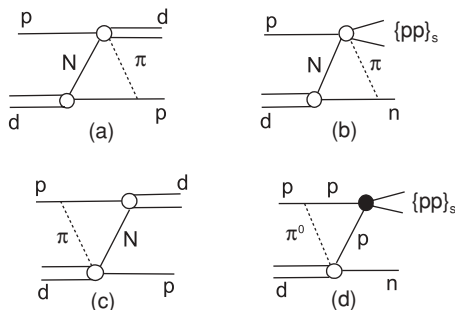FIG. 19. Mechanisms of the $pd \to dp$ (a, c) and $pd \to \{pp\}_s n$ (b, d) processes for the OPE-I (a, b) and OPE-II (c, d) models.

within the ONE + SS + Δ approach. The OPE-II model yields for the ratio of the $pd \to \{pp\}_s n$ and $pd \to dp$ cross sections [Eq. (4)] $r^{\text{th}} = 0.016$–0.013. This is in qualitative agreement with the experimental value of $r^{\text{exp}} = 0.009$–0.011, found for the $pd \to dp$ and $pd \to \{pp\}_s n$ data [38,44–47,50]. The larger probability for the formation of a deuteron compared to the $\{pp\}_s$ diproton is naturally explained within this model. It is a consequence of several reasons, including spin-isospin, combinatorial, and phase-space factors; the ratio of the relevant nuclear form factors enters as well.

At higher energies, the role of heavier nucleon isobars in the subprocesses $\pi^+ d \to pp$ and $\pi d \to pn$ increases [69,70]. As a result, the OPE model shows a decrease of the slope in the energy dependence of the cross sections of the $pd \to dp$ and $pd \to \{pp\}_s n$ reactions at about 1.5 GeV. This tendency is in qualitative agreement with pd elastic data and the new data on $pd \to \{pp\}_s n$ obtained in this work. However, the OPE model underestimates sizeably the absolute value of the cross section above 1 GeV for both the $pd \to dp$ and $pd \to \{pp\}_s n$ reactions, indicating that contributions from other mechanisms are also relevant in this region. According to Ref. [67], agreement with the data on $pd \to \{pp\}_s n$ can be improved by taking into account the ONE mechanism in addition to OPE, although one should note that this procedure is problematic due to double counting.

At last, a successful description of the data on the unpolarized cross section, tensor analyzing power T_{20}, and polarization transfer κ^0 in pd backward elastic scattering in the energy range from 0.5 to 2.7 GeV was obtained recently [71] within the OPE model plus ONE mechanism considered within a covariant form of relativistic dynamics [72]. It would be very instructive to further develop and to apply this approach [71] to the analysis of the $pd \to \{pp\}_s n$ reaction.

C. Other approaches

Here we consider other approaches to the $pd \to \{pp\}_s n$ reaction that were stimulated by the ANKE data.

1. Bethe-Salpeter approach

With increasing beam energy, relativistic effects become more important in the $pd \to \{pp\}_s n$ reaction. In the $ONE + SS + \Delta$ approach, these effects have been taken into account within a relativistic Hamiltonian dynamics, developed for systems with a fixed number of particles [73]. A fully covariant approach based on the spinor-spinor Bethe-Salpeter equation with a realistic one-boson-exchange kernel in the ladder approximation was applied in Ref. [74] to the analysis of the $pd \to \{pp\}_s n$ reaction, and a rather good agreement with the data of Ref. [25] was achieved. The FSI effects have been taken into account in the pp pair by treating it as a relativistic $^1S_0$ scattering state. A rather important contribution of the Lorentz-boost effects and relativistic P waves in the pp system has been found. This results in the shifting of the minimum and removal of the dip in the ONE cross section caused by the repulsion in the $^1S_0$ pp interaction. The inclusion of P-wave components corresponds to the involvement of intermediate $\overline{N}NNN$ states, which can be compared with the effects of pair meson-exchange currents and isobar

contributions in nonrelativistic calculations. The $N\Delta N$ configurations taken into account within the $ONE + SS + \Delta$ approach in Refs. [26,67] were found to dominate in the $pd \to \{pp\}_s n$ reaction at about 0.6–1.2 GeV, but were not considered in Ref. [74].

2. Constituent counting rules

At asymptotically high energies $\sqrt{s}$ and transferred momenta t, dimensional analyses [75,76] and perturbative QCD [77,78] lead to constituent quark counting rules (CCR) for exclusive binary reactions, $d\sigma/dt \sim s^{-n} f(\frac{t}{s})$, where $n + 2$ is the total number of point-like objects in the initial and final states. The s^{-n} dependence was observed for many reactions with free hadrons at moderate energies and large fixed scattering angles (see, for example, Ref. [79]).

For reactions with nuclei, the CCR behavior of the cross section would be considered as an indication of a transition region from hadron to quark degrees of freedom. As in the case of electromagnetic form factors and two-body hadronic reactions, the scale for the onset of the CCR regime cannot be predicted theoretically and must be determined experimentally. At SLAC and JLab, the CCR behavior was observed in the region of 1 GeV in deuteron photodisintegration $\gamma d \to pn$ (see Ref. [80] and references therein). A recent analysis of available data on pure hadronic reactions, that is, $dd \to {}^3\mathrm{H}p$ and $dp \to dp$ at large fixed scattering angles $\theta_{cm} \sim 60°$–$90°$ also shows a similar onset of CCR scaling in the GeV region [81]. The internal nucleon momenta that correspond to the observed onset of CCR scaling are about $1\,\mathrm{GeV}/c$ for the $\gamma d \to pn$ reaction and $\sim 0.5\,\mathrm{GeV}/c$ in the $dd \to {}^3\mathrm{H}p$ and $dp \to dp$ reactions. These large momenta reflect the hardness of those reactions and can be considered as a criterion for the scaling regime.

The $pd \to \{pp\}_s n$ and the $pd \to dp$ processes are considered here at energies that are very far from those where CCR are usually applied. Nevertheless, in the region between the $\Delta(1232)$ and $\Delta(1920)$ resonances, a test for a possible CCR scaling behavior is meaningful, because the internal momenta in the deuteron and the diproton in these reactions reach large values of $q \sim 0.5\,\mathrm{GeV}/c$. (For the ONE mechanism, this corresponds to $T_p = 1.5$ GeV.) In both reactions, the total number of quarks in the initial and final states is 18; therefore one should expect an exponent of $n = 16$. A fit in the energy range $T_p = 1$–2 GeV to the $pd \to dp$ data and the previously published $pd \to \{pp\}_s n$ data [25] at $\theta_{cm} = 172°$–$180°$ gave an exponent of $n \simeq 12.9$ [67]. The deviation from the expected asymptotic value $n = 16$ was attributed to diquark-cluster configurations in free nucleons of deuteron and diproton. If the momentum transfer is not large enough to resolve the intrinsic structure of the diquarks, these would act as point-like objects, thereby lowering the expected exponent n.

Our fits, shown in Fig. 20, were performed at fixed angle $\theta_{cm} = 180°$ in the region 0.95–2 GeV and yield exponents of $n = 11.88 \pm 0.53$ ($\chi^2/\mathrm{ndf} = 56/4$) for the $pd \to \{pp\}_s n$ reaction and $n = 11.70 \pm 0.32$ ($\chi^2/\mathrm{ndf} = 18/9$) for the $pd \to dp$ process. Since the χ^2/ndf are rather large,
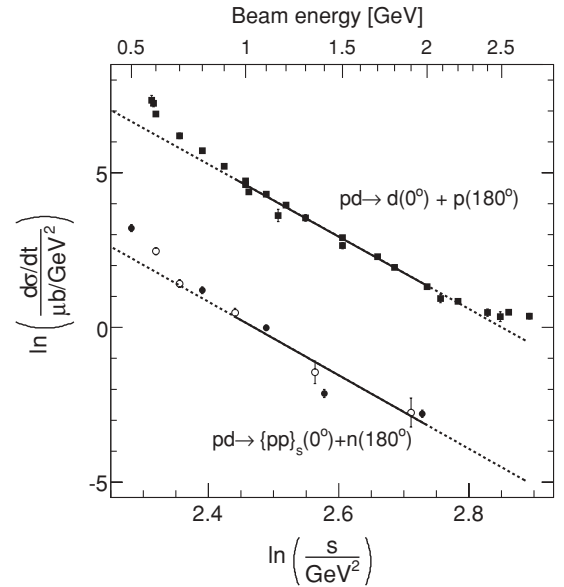

FIG. 20. Differential cross section $\ln(d\sigma/dt)$ as a function of $\ln(s)$ for pd backward elastic scattering and the $pd \to \{pp\}_s n$ reaction. The previously obtained data of Ref. [25] are shown by open circles ($\circ$), and the new data are shown by bullets ($\bullet$). The fits in the range 0.95–2.0 GeV for pd backward elastic scattering and $pd \to \{pp\}_s n$ yield exponents of $n = 11.70 \pm 0.32$ ($\chi^2/\mathrm{ndf} = 18/9$) and $n = 11.88 \pm 0.53$ ($\chi^2/\mathrm{ndf} = 56/4$), respectively. The upper scale indicates the incident proton beam energy.

realistic uncertainties of the two exponents are considerably larger by factors of 4 and 2, respectively, compared to those listed previously. The obtained exponents are within errors the same for both reactions, and are in the CCR ballpark. Here we recall that CCR experiments for πN, KN, $\bar{K}N$, and NN scattering have been confirmed within 1–1.5 units [79].

D. Related topics

The study of hard pd interactions in the GeV region induced in the past several fruitful ideas. When studying the quasielastic knock-out of fast deuterons from nuclei by protons at 675 MeV, for instance, a hypothesis about density fluctuations of nuclear matter was supposed in Ref. [82]. This idea stimulated an intensive search for flucton (or, in modern language, multiquark configurations) in nuclei and led to the observation of cumulative effects [4] (for a recent review, see Ref. [5]). The possibility to search for NN^* components in the deuteron had been related also to pd backward elastic scattering [83]. Furthermore, the possible formation of other exotic objects in the intermediate state, like three-baryon resonances [17] and color strings [84], was also discussed in conjunction with pd backward elastic scattering in the GeV region.

The contribution of these ingredients, however, is strongly model dependent and, despite the many efforts undertaken, well-established results were not obtained. However, the excitation of well-known resonances, like the Δ isobar, plays an important role in these collisions. The expected contribution

of three-baryon resonances, introduced as an attempt to solve the T_{20} puzzle in pd backward elastic scattering, was significantly reduced after a more careful analysis of the $\Delta(1232)$ isobar contribution was carried out [85]. The Δ-isobar excitation, caused by the long- and medium-range interaction, complicates the study of short-range properties of few-nucleon systems. Studies of the breakup reaction with a diproton in the final state, in which the Δ and N^* contributions are suppressed by isospin invariance, could reveal the aforementioned aspects of the short-range dynamics in pd collisions.

The results of the analysis performed within the conventional meson-baryon picture in this work and in Ref. [26] show that non-nucleonic degrees of freedom yield rather small contributions in the GeV region. At moderate energies, but large enough to test the region of the NN core via the ONE mechanism, the agreement between theory and data on unpolarized cross sections can be considered to be almost quantitative. The $\Delta(1232)$ still dominates at these energies. This mechanism realizes the contribution of a special type of three-body force, whose relative contribution at lower energies is much smaller and rather uncertain [20,86]. One may conclude that the $pd \rightarrow \{pp\}_s n$ reaction at 0.5–1.0 GeV offers a new tool for the study of this type of three-body force, as discussed in Ref. [87]. At higher energies the agreement is worse; nevertheless, one observes that better phenomenological NN potentials lead to a better agreement with the experimental data on the $pd \rightarrow \{pp\}_s n$ reaction [26]. In general, three-body reactions allow one to test those properties of the interaction between nucleons that are absent in two-body NN data, for example, high-momentum components of the NN wave functions and three-body forces. As suggested in Ref. [26] and confirmed here by the more precise new data, high-momentum components in the deuteron and the diproton appear to be rather weak.

Very similar arguments were applied to motivate investigations of other reactions with the formation of a diproton in the final state [88–90]. These are $pp \rightarrow \{pp\}_s \pi^0$ and $pp \rightarrow \{pp\}_s \gamma$, investigated at several hundred MeV in kinematics of $pp \rightarrow d\pi^+$ and $pn \rightarrow d\gamma$, respectively. Like in the present study, the Δ-isobar contributions were expected to be significantly suppressed compared to the corresponding reactions with a final deuteron due to general symmetry properties. But the measurements [88–90] show pronounced enhancements of the cross sections in the Δ region. Presumably, these results also indicate that high-momentum components in the NN wave functions are rather weak [91].

Under the assumption that the ONE mechanism dominates at energies above the $\Delta(1232)$-isobar region ($T_p > 1.5$ GeV) the observed small ratio $r \approx 10^{-2}$, given in Eq. (4), implies that triplet pn pairs (deuterons) with high internal momenta $q = 0.5$–0.6 GeV/c occur much more often than singlet $\{pp\}_s$ pairs. A similar finding was recently reported with respect to correlated NN pairs in nuclei [6] in the analysis of nuclear reactions (p, ppn) in Refs. [92,93] and in the $(e, e'pp)$ and $(e, e'pn)$ reactions at high transferred momenta [94]. Calculations of two-nucleon momentum distributions for the ground states of the lightest nuclei are in agreement with this conjecture [95].

V. SUMMARY AND CONCLUSIONS

The $pd \rightarrow \{pp\}_s n$ reaction has been studied in the energy range 0.5–2.0 GeV in a kinematics similar to that of pd backward elastic scattering. The cross section of the deuteron breakup reaction with a diproton in the final state was found to be about two orders of magnitude smaller than the latter. The high statistics obtained at beam energies of 0.5, 0.8, 1.1, 1.4, and 1.97 GeV allowed us to determine the dependence of the differential cross section on the diproton excitation energy E_{pp}, on the proton emission angle θ_k in the rest frame of the proton pair, and on the neutron emission angle θ_n. For E_{pp} less than 3 MeV the distributions of E_{pp} (Fig. 10) and θ_k (Fig. 11) are caused by the final-state interaction between the protons and are used here to validate the dominance of the $^1S_0$ pp state.

The shape of the energy dependence of the measured differential cross section of the $pd \rightarrow \{pp\}_s n$ reaction obtained at $\theta_n = 180°$ is similar to the one of pd backward elastic scattering. Both processes exhibit a decrease of the cross section in the energy range $\sim$0.7–1.4 GeV by one order of magnitude with a smaller decrease at the higher energies. In the angular range from 168° to 180° the differential cross sections change smoothly with θ_n and exhibit only a small variation of the slope near $\theta_n = 180°$ as a function of energy.

The theoretical analysis shows that the ONE + SS + Δ model with rescatterings in the initial and final states allows one to describe reasonably well the obtained $pd \rightarrow \{pp\}_s n$ differential cross section when a rather soft short-distance NN potential is used, like the CD-Bonn potential. The results of calculations [26] performed within the same model, but with harder NN potentials, like the Paris or the RSC potentials, are clearly contradicting the data. This observation, first described in Ref. [26] and confirmed here by the new high-statistics data, constitutes the most important finding of the study of the $pd \rightarrow \{pp\}_s n$ reaction.

The excitation of a $\Delta(1232)$ in the intermediate state represents a contribution of a three-body force to the $pd \rightarrow \{pp\}_s n$ reaction. This contribution turned out to become important at energies of 0.54–1.0 GeV due to the node in the ONE amplitude (see Fig. 16), located in this reaction at $\approx$0.8 GeV, which is caused by the repulsive NN core in the $^1S_0$ state. One should note, however, that neither the Δ mechanism alone nor the separate ONE mechanism provides an agreement with the experimental data below 1 GeV. Only their coherent sum allows one to describe the data. An analysis within the OPE model with the subprocess $\pi^0 d \rightarrow pn$ confirms independently the dominance of the $\Delta(1232)$ isobar contribution at energies below 1 GeV. Above 1 GeV, the OPE model accounts for the contribution of heavier nucleon isobars, but underestimates the absolute value of the measured cross section at $\sim$1–2 GeV. In accordance with the results of the ONE + SS + Δ calculations, this implies that the ONE contribution cannot be neglected at higher energies of 1–2 GeV.

In view of high internal momenta $q \sim 0.5$–0.6 GeV/c probed by the ONE mechanism in this energy region, it is important to gain more insight into the ONE contribution by independent measurements. The planned measurements of the tensor analyzing power T_{20} and spin correlation $C_{y,y}$ of the

$\vec{p}\vec{d} \rightarrow \{pp\}_s n$ reaction could clarify further the underlying dynamics of this process and shed light on the role of the ONE mechanism [96].

APPENDIX: CONTRIBUTION OF P WAVES TO ONE

We write the deuteron breakup reaction $pd \rightarrow \{pp\}_s n$ with the c.m. three-momenta and polarizations indicated in parentheses,

$$p(\mathbf{p}_1, \sigma_1) + d(\mathbf{P}_d, \lambda_d) \rightarrow p(\mathbf{p}'_1, \sigma'_1) + p(\mathbf{p}'_2, \sigma'_2) + n(\mathbf{p}_n, \sigma_n). \quad (A1)$$

The general expression for the invariant cross section of the reaction is

$$d\sigma = (2\pi)^4 \delta^4(P_i - P_f) \frac{1}{4I} \overline{|A_{fi}|}^2$$
$$\times \frac{d^3 p'_1}{2E'_1 (2\pi)^3} \frac{d^3 p'_2}{2E'_2 (2\pi)^3} \frac{d^3 p_n}{2E_n (2\pi)^3}. \quad (A2)$$

$\overline{|A_{fi}|}^2$ denotes the squared spin-averaged reaction amplitude, and P_i and P_f are the total four-momenta of the initial and final system of particles, respectively. $I = \sqrt{(E_1 E_d - \mathbf{p}_1 \mathbf{P}_d)^2 - m^2 M_d^2}$, where M_d and m are the masses of the deuteron and the nucleon, $E_i = \sqrt{\mathbf{p}_i^2 + m^2}$, $E'_i = \sqrt{\mathbf{p}_i'^2 + m^2}$, and $E_d = \sqrt{\mathbf{P}_d^2 + M_d^2}$. Integrating Eq. (A2) over the three-momentum $\mathbf{p}'_2$ and the energy E_n, the differential cross section reads

$$\frac{d\sigma}{dk^2 d\Omega_\mathbf{k} d\Omega_n} = \frac{p_n}{p_1} \frac{k}{(4\pi)^5 s E_k} \overline{|A_{fi}|}^2. \quad (A3)$$

Here $\mathbf{k}$ denotes the relative momentum in the final proton pair, $E_k = k^2/m$ is the kinetic energy in the c.m. system of the pair, and s is the invariant mass of the $p + d$ system. To obtain the differential cross section $d\sigma/d\Omega_n$, one has to integrate Eq. (A3) over k^2 from 0 to the maximum momentum squared k_{max}^2 and over all directions of the momentum $\mathbf{k}$. Due to the identity of the final protons, when performing integration over $d\Omega_\mathbf{k}$ within the full 4π solid angle, the right-hand side of Eq. (A3) has to be multiplied by a factor of $\frac{1}{2}$.

Only the $^1S_0$ state of the final pp pair was taken into account in Ref. [26]. In the following, we evaluate the contribution of P waves in the final state of the two protons under the assumption that only the ONE mechanism is present in the $pd \rightarrow \{pp\}_s n$ reaction. According to Ref. [22] where a general formalism for this mechanism was developed in the plane wave

approximation, the spin-averaged squared matrix element can be written as

$$\overline{|A_{fi}|}^2 = \frac{1}{6} \sum_{\lambda_d \sigma_1 \sigma'_1 \sigma'_2 \sigma_n} |A_{fi}|^2$$
$$= \frac{E_d(E_2 + E'_n)\varepsilon_p(q)}{16\pi E_2^2} \left[u_0^2(q) + u_2^2(q) \right] F(\mathbf{q}', \mathbf{k}). \quad (A4)$$

Here $\varepsilon_p(q) = \sqrt{m^2 + q^2}$; $u_0(q)$ and $u_2(q)$ are the S- and D-wave components of the deuteron wave function; E_d, E_2, and E_n are the total energies of the deuteron, the intermediate proton, and the final neutron in the c.m. system of the reaction; q is the internal momentum in the deuteron; and q' is the off-shell relative momentum in the proton pair and k its on-shell momentum. The internal momenta q and q' are related to the momenta of initial and final particles according to the relativistic kinematics. The function $F(\mathbf{q}', \mathbf{k})$ can be written via the amplitude of elastic pp scattering $T_{pp}(\mathbf{q}', \mathbf{k})$ in the form

$$F(\mathbf{q}', \mathbf{k}) = \sum_{\substack{\sigma'_1 \sigma'_2 \\ \sigma_1 \sigma_2}} \left| T_{NN\sigma_1\sigma_2}^{\sigma'_1\sigma'_2}(\mathbf{q}', \mathbf{k}) \right|^2$$
$$= \sum_{JLL'\widetilde{J}\widetilde{L}\widetilde{L}'Sl} \mathcal{N}_{pp}^2(L, S) t_{LL'}^{JS}(q', k)\left(t_{\widetilde{L}\widetilde{L}'}^{\widetilde{J}S}(q', k)\right)^*$$
$$\times C_{L0l0}^{\widetilde{L}0} C_{L'0l0}^{\widetilde{L}'0}(2J + 1)(2\widetilde{J} + 1)(2l + 1)$$
$$\times \sqrt{(2L+1)(2L'+1)} \begin{Bmatrix} \widetilde{L} & L & l \\ J & \widetilde{J} & S \end{Bmatrix} \begin{Bmatrix} \widetilde{L}' & L' & l \\ J & \widetilde{J} & S \end{Bmatrix}$$
$$\times P_l(\mathbf{q}'\mathbf{k}/q'k), \quad (A5)$$

where $N_{pp}(L, S) = 1 + (-1)^{L+S}$ is the combinatorial factor for two protons; the braces stand for the usual notation of $6j$ symbols. $C_{LMlm}^{JM_J}$ is the Clebsh-Gordan coefficient, and P_l is the Legendre polynomial of lth order. $t_{LL'}^{JS}(q', k)$ is the partial t matrix of pp scattering for the transition $L \rightarrow L'$ in the state with spin S and total angular momentum J. The function $F(\mathbf{q}', \mathbf{k})$ in Eq. (A5) at $q' = k$ describes the differential cross section of pp scattering. As seen from Eq. (A5), the states with different spins S do not interfere in the cross section. This is a consequence of the total angular momentum J and parity conservation. Therefore, it is reasonable to separate transitions in singlet ($S = 0$) and triplet ($S = 1$) channels.

Let us now consider the relative contributions of the spin-singlet $^1S_0$ and spin-triplet waves $^3P_0$, $^3P_1$, and $^3P_2$ for $E_{pp}^{max} = 3$ MeV. For simplicity, we consider collinear kinematics with $\theta_n = 180°$. In this case, the direction of the vector $\mathbf{q}'$ coincides with the beam direction; therefore, the angle between $\mathbf{q}'$ and $\mathbf{k}$ is equivalent to θ_k, which is the angle between $\mathbf{k}$ and the total diproton momentum. Thus, the squared transition matrix element in Eq. (A4) can be written as

$$\overline{|A_{fi}|}^2 = \sum_l C_l(2l + 1)P_l(\cos\theta_k), \quad (A6)$$

where the coefficients C_l can be deduced from Eq. (A5). The angular momentum l takes the values 0, 1, or 2. One can find that $l = 0$ corresponds to the following combinations of partial t matrices $t_{LL'}^{JS}(q', k)$: $^1S_0 \times {}^1S_0$, $^3P_0 \times {}^3P_0$, $^3P_1 \times {}^3P_1$, and $^3P_2 \times {}^3P_2$, each of them leading to an isotropic distribution

over $\cos\theta_k$. The value $l = 1$ corresponds to the combinations $^3P_0 \times {}^3P_1$, $^3P_1 \times {}^3P_0$, $^3P_1 \times {}^3P_1$, $^3P_1 \times {}^3P_2$, $^3P_2 \times {}^3P_1$, and $^3P_2 \times {}^3P_2$. At last, $l = 2$ comes from the combinations $^3P_1 \times {}^3P_1$, $^3P_1 \times {}^3P_2$, $^3P_2 \times {}^3P_1$, and $^3P_2 \times {}^3P_2$. One can see from Eq. (A4) that for P waves the Clebsh-Gordan coefficients $C_{L0l0}^{\tilde{L}0}$ and $C_{L'0l0}^{\tilde{L}'0}$ are reduced to $C_{1010}^{10} = 0$. Therefore, the coefficient in front of $P_1(\cos\theta)$ in Eqs. (A4) and (A6) reads $C_1 = 0$. The only nonisotropic term for the ONE mechanism is given by $l = 2$. In a numerical calculations for the $^1S_0$- and P-wave scattering amplitudes, we used separable representations of the t matrices from Ref. [97] obtained for the CD-Bonn potential. At

$E_{pp} = 3$ MeV and $l = 2$, we found the following ratios at the different beam energies, $C_2/C_0 = 0.0022$ (0.5 GeV), 0.0748 (0.8 GeV), 0.0164 (1.1 GeV), 0.0048 (1.4 GeV), and 0.002 (1.97 GeV). The experimentally determined ratios C_2/C_0 are listed in Table IV. The P-wave contributions to the isotropic part of the squared matrix element of Eq. (A6), that is, to the coefficient C_0, are 0.007, 0.229, 0.053, 0.016, and 0.007 at the same energies. The large increase of the C_2/C_0 ratio at 0.8 GeV originates from the vanishing half-off shell $t(q, k)(^1S_0)$ matrix at this energy, but does not occur in the other mechanisms, where such nodes do not exist.

---

[1] R. Gilman and F. Gross, J. Phys. G: Nucl. Part. Phys. **28**, R37 (2002).

[2] M. Garçon and J. W. Van Orden, Adv. Nucl. Phys. **26**, 293 (2001).

[3] C. Bochna *et al.*, Phys. Rev. Lett. **81**, 4576 (1998), see also Refs. [3], [4], [9], and [10] therein.

[4] A. M. Baldin, Nucl. Phys. A **434**, 659 (1985).

[5] G. A. Leksin, Yad. Fiz. **65**, 2042 (2002) [Phys. Atom. Nucl. **65**, 1985 (2002)].

[6] M. I. Strikman and L. L. Frankfurt, Phys. Rep. **76**, 215 (1981).

[7] L. Frankfurt, M. Sargsian, and M. Strikman, Int. J. Mod. Phys. A **23**, 2991 (2008).

[8] V. Punjabi *et al.*, Phys. Lett. B **350**, 178 (1995).

[9] L. S. Ahzgirey *et al.*, Phys. Lett. B **391**, 22 (1997); Yad. Fiz. **61**, 494 (1998) [Phys. At. Nucl. **61**, 432 (1998)].

[10] V. G. Ableev *et al.*, Nucl. Phys. A **393**, 491 (1983).

[11] C. F. Perdrisat *et al.*, Phys. Rev. Lett. **59**, 2840 (1987).

[12] L. S. Azhgirey *et al.*, Phys. Lett. B **387**, 37 (1996).

[13] See, for example, E. Strokovsky, Yad. Fiz **62**, 1193 (1999) [Phys. Atom. Nucl. **62**, 1120 (1999)].

[14] M. Lacombe *et al.*, Phys. Lett. B **101**, 139 (1981).

[15] R. V. Reid Jr., Ann. Phys. (NY) **50**, 411 (1968).

[16] J. Arvieux *et al.*, Nucl. Phys. A **431**, 613 (1984).

[17] L. A. Kondratyuk, F. M. Lev, and L. V. Schevchenko, Yad. Fiz. **33**, 1208 (1981) [Sov. J. Nucl. Phys. **33**, 642 (1981)].

[18] A. Boudard and M. Dillig, Phys. Rev. C **31**, 302 (1985).

[19] Yu. N. Uzikov, Fiz. Elem. Chastits At. Yadra **29**, 1405 (1998) [Phys. Part. Nucl. **29**, 583 (1998)].

[20] K. Sekiguchi *et al.*, Phys. Rev. C **65**, 034003 (2002).

[21] O. Imambekov and Yu. N. Uzikov, Yad. Fiz. **52**, 1361 (1990) [Sov. J. Nucl. Phys. **52**, 862 (1990)].

[22] A. V. Smirnov and Yu. N. Uzikov, Yad. Fiz. **61**, 421 (1998) [Phys. At. Nucl. **61**, 361 (1998)].

[23] Yu. N. Uzikov, J. Phys. G: Nucl. Part. Phys. **28**, B13 (2002).

[24] Yu. Uzikov, Pis'ma Zh. Eksp. Teor. Fiz. **75**, 7 (2002) [JETP Lett. **75**, 5 (2002)].

[25] V. I. Komarov *et al.*, Phys. Lett. B **553**, 179 (2003).

[26] J. Haidenbauer and Yu. Uzikov, Phys. Lett. B **562**, 227 (2003).

[27] R. Machleidt, Phys. Rev. C **63**, 024001 (2001).

[28] S. Barsov *et al.*, Nucl. Instrum. Methods A **462**, 364 (2001).

[29] R. Maier, Nucl. Instrum. Methods A **390**, 1 (1997).

[30] A. Khoukaz *et al.*, Eur. Phys. J. D **5**, 275 (1999).

[31] S. Dymov *et al.*, Part. Nucl. Lett. **119**(2) 40 (2003).

[32] S. Dymov *et al.*, Comm. JINR, Dubna, E10-2002-19 (2002).

[33] S. Yaschenko *et al.*, Phys. Rev. Lett. **94**, 072304 (2005).

[34] B. Chiladze *et al.*, Part. Nucl. Lett. **113**(4), 95 (2002).

[35] S. Agostinelli *et al.*, Nucl. Instrum. Methods A **506**, 250 (2003).

[36] V. Franko and R. J. Glauber, Phys. Rev. **142**, 1195 (1966).

[37] A. G. Sitenko, Fiz. Elem. Chastits At. Yadra **4**, 547 (1973) [Sov. J. Part. Nucl. **4**, 231 (1973)].

[38] E. T. Boschitz *et al.*, Phys. Rev. C **6**, 457 (1972).

[39] O. G. Grebenjuk *et al.*, Nucl. Phys. A **500**, 637 (1989).

[40] F. Irom, G. J. Igo, J. B. McClelland, C. A. Whitten, and M. Bleszynski, Phys. Rev. C **28**, 2380 (1983).

[41] N. Dalkhazov *et al.*, Yad. Fiz. **8**, 342 (1968).

[42] B. S. Aladashvili *et al.*, J. Phys. G: Nucl. Phys. **3**, 1 (1977).

[43] S. Yaschenko, Ph.D. thesis, University of Erlangen, Germany, 2004. Available from http://www.fz-juelich.de/ikp/anke/en/theses/S.Yaschenko_PhD.pdf.

[44] J. C. Alder *et al.*, Phys. Rev. C **6**, 2010 (1972).

[45] N. E. Booth *et al.*, Phys. Rev. D **4**, 1261 (1971).

[46] E. Winkelman, P. R. Bevington, M. W. McNaughton, H. B. Willard, F. H. Cverna, E. P. Chamberlin, and N. S. P. King, Phys. Rev. C **21**, 2535 (1980).

[47] L. Dubal *et al.*, Phys. Rev. D **9**, 597 (1974).

[48] A. Boudard, Thesis, CEA-N-2386, Saclay, 1984.

[49] B. E. Bonner *et al.*, Phys. Rev. C **17**, 671 (1978).

[50] P. Berthet *et al.*, J. Phys. G: Nucl. Phys. **8**, L111 (1982).

[51] R. A. Arndt, I. I. Strakovsky, R. L. Workman, and D. V. Bugg, Phys. Rev. C **48**, 1926 (1993).

[52] M. Akemoto *et al.*, Phys. Lett. B **149**, 321 (1984).

[53] K. M. Watson, Phys. Rev. **88**, 1163 (1952).

[54] A. B. Migdal, Zh. Eksp. Theor. Fiz. **28**, 3 (1953).

[55] B. J. Morton *et al.*, Phys. Rev. **169**, 825 (1968).

[56] C. Hanhart and K. Nakajama, Phys. Lett. B **454**, 176 (1999).

[57] V. V. Baru *et al.*, Phys. At. Nucl. **64**, 579 (2001).

[58] J. D. Jackson and J. M. Blatt, Rev. Mod. Phys. **22**, 77 (1950).

[59] R. D. Felder *et al.*, Nuc. Phys. A **280**, 308 (1977).

[60] Yu. Uzikov *et al.*, Eur. Phys. J. A **18**, 317 (2003).

[61] Yu. N. Uzikov, Yad. Fiz. **60**, 1603 (1997) [Phys. At. Nucl. **60**, 1458 (1997)].

[62] J. Hudomaly-Gabitzsch, I. M. Duck, M. Furic, G. S. Mutchler, J. M. Clement, R. D. Felder, W. H. Dragoset, G. C. Phillips, J. C. Allred, E. V. Hungerford, B. W. Mayes, L. S. Pinsky, and T. M. Williams, Phys. Rev. C **18**, 2666 (1978).

[63] O. Imambekov, Yu. N. Uzikov, Yad. Fiz. **47**, 1089 (1988) [Sov. J. Nucl. Phys. **47**, 695 (1988)].

[64] B. J. Verwest, Phys. Lett. B **83**, 161 (1979).

[65] S. J. Wallace, Adv. Nucl. Phys. **12**, 135 (1981).

[66] The ONE mechanism could provide a negative slope of the angular dependence at energies just above the ONE node [21]. However, to explain the observed angular dependence at 1.1–1.4 GeV, the calculated ONE cross section has to be rather large,

which would suggest high-momentum components of the NN wave function that are too large, which is in contradiction with Ref. [26].

[67] Yu. N. Uzikov, J. Haidenbauer, and C. Wilkin, Phys. Rev. C **75**, 014008 (2007).

[68] N. S. Cragie and C. Wilkin, Nucl. Phys. B **14**, 477 (1969).

[69] D. Dekkers *et al.*, Phys. Lett. **11**, 161 (1964).

[70] M. Akemoto *et al.*, Phys. Lett. B **149**, 321 (1984).

[71] A. P. Ierusalimov, G. I. Lykasov, and M. Viviani, Few-Body Syst. **44**, 315 (2008).

[72] W. W. Buck and F. Gross, Phys. Rev. D **20**, 2361 (1979).

[73] B. L. G. Bakker, L. A. Kondratyuk, and M. V. Terentjev, Nucl. Phys. B **158**, 497 (1979).

[74] L. P. Kaptari *et al.*, Eur. Phys. J. A **19**, 301 (2004).

[75] A. V. Matveev, R. M. Muradyan, and A. N. Tavkhelidze, Lett. Nuovo Cimento **7**, 719 (1973).

[76] S. J. Brodsky and G. R. Farrar, Phys. Rev. Lett. **31**, 1153 (1973).

[77] G. P. Lepage and S. J. Brodsky, Phys. Rev. D **22**, 2157 (1980).

[78] A. V. Efremov and A. V. Radyushkin, Phys. Lett. B **94**, 245 (1980); Theor. Math. Phys. **42**, 97 (1980).

[79] C. White *et al.*, Phys. Rev. D **49**, 58 (1994).

[80] P. Rossi *et al.*, Phys. Rev. Lett. **94**, 012301 (2005).

[81] Yu. N. Uzikov, Pis'ma Zh. Exp. Theor. Phys. **81**, 387 (2005) [JETP Lett. **81**, 387 (2005)].

[82] D. I. Blokhintsev, J. Exp. Theor. Phys. **33**, 1295 (1957); Sov. Phys. JETP **6 (33)**, 995 (1958).

[83] A. Kerman and L. Kisslinger, Phys. Rev. **180**, 1483 (1969).

[84] B. Z. Kopeliovich and F. Niedermayer, Phys. Lett. B **117**, 101 (1982); Sov. Phys. JETP **60**, 640 (1984).

[85] O. Imambekov, Yu. N. Uzikov, and L. V. Schevschenko, Z. Phys. A **322**, 349 (1989).

[86] H. Witala *et al.*, Phys. Rev. C **73**, 044004 (2006).

[87] Yu. N. Uzikov, Few-Body Syst. **44**, 211 (2008).

[88] S. Dymov *et al.*, Phys. Lett. B **635**, 270 (2006).

[89] V. Kurbatov *et al.*, Phys. Lett. B **661**, 22 (2008).

[90] V. Komarov *et al.*, Phys. Rev. Lett. **101**, 102501 (2008).

[91] Yu. N. Uzikov, in *Proceedings of the XIX International Baldin Seminar on High Energy Physics Problem (September 2008, Dubna)*, edited by A. N. Sissakian, V. V. Burov, A. I. Malakhov, S. G. Bandarenko, and E. B. Plekhanov (Joint Institute for Nuclear Research, Dubna, Russia, 2009), Vol. 2, p. 307.

[92] A. Tang *et al.*, Phys. Rev. Lett. **90**, 042301 (2003).

[93] E. Piasetzky, M. Sargsian, L. Frankfurt, M. Strikman, and J. W. Watson, Phys. Rev. Lett. **97**, 162504 (2006).

[94] R. Shneor *et al.*, Phy. Rev. Lett. **99**, 072501 (2007).

[95] R. Schiavilla *et al.*, Phys. Rev. Lett. **98**, 132501 (2007).

[96] A. Kacharava, F. Rathmann, and C. Wilkin, arXiv:nucl-ex/0511028.

[97] V. Lensky *et al.*, Eur. Phys. J. A **26**, 107 (2005).